

Robust output-feedback VFO-ADR control of underactuated spatial vehicles in a task of following the non-parametrized path

Krzysztof Łakomy*, Maciej Marcin Michałek

Institute of Automation and Robotics, Poznan University of Technology (PUT), Piotrowo 3A, 60-965 Poznań, Poland

Abstract

This article concerns the development of the Vector Field Orientation - Active Disturbance Rejection (VFO-ADR) cascaded path-following controller for the underactuated vehicles moving in a 3-dimensional space. The proposed concept of a cascaded control structure decouples system kinematics from system dynamics, resembling the approach utilized in the nonholonomic systems. Thanks to the use of an ADR control approach in the dynamic-level controller, the proposed control structure is robust to even significant model uncertainties and external disturbances. Application of an error-based form of the Extended State Observer (ESO), implemented within the ADR inner-loop controller, implies the output-feedback characteristic of the control structure, i.e., only the position and attitude of the vehicle body is expected to be measured. The kinematic-level controller is designed according to the VFO method utilizing the non-parametrized path representation to calculate the commanded velocities. The description of the proposed control structure is followed by the theoretical analysis utilizing the Input-to-State Stability (ISS) theorem and the simulation verification of the proposed solution.

Keywords: VFO, ADRC, robust control, output-feedback, path following, cascaded control, underactuated vehicle

1. Introduction

The interest in automatic control of Unmanned Aerial Vehicles (UAVs) and Autonomous Underwater Vehicles (AUVs) has been gradually growing in recent years, and resulted in a large amount of the designed control structures for various types of objects, such as multicopters [34, 31, 29, 39], airships [46, 45, 37, 2], fixed-wing planes [17] or underwater exploring robots [6, 14, 30]. Looking throughout the control architectures proposed in the literature, one can observe that the controllers intended for the mobile robots are most frequently focused on solving one (or more) of three classical motion tasks, i.e., path-following [3, 44, 32, 11, 45, 41], trajectory tracking [14, 1] or set-point stabilization [2, 7]. All of the aforementioned control tasks have been solved utilizing various control methods, like backstepping [2, 3], model predictive control [17], sliding mode control [43] or active disturbance rejection control [46, 39], each having specific properties suited for a particular application.

The movement of spatial vehicles can be performed with three different motion strategies. The least common omnidirectional motion [5, 24] can be applied only to fully-actuated vehicles that can generate substantial forces in every Degree of Freedom (DoF). The actuation systems implemented on the aerial/underwater vehicles are usually capable of executing large control signals only in some distinguished directions,

making it necessary to use one of the other available motion strategies. Alternative approaches to the omnidirectional movement are, for example, the unicycle-like and the torpedo-like motion strategies, both relying on the motion realization along with some privileged directions, aligned with the thrust generated by the main actuators. In the unicycle-like motion, the vehicle movement is decomposed into the planar, and fully decoupled vertical motions [45, 32, 46], while in the torpedo-like approach the control object moves directly in the 3d space [14, 28, 11, 33]. A specific actuation strategy utilized for the vehicles that are usually moving in a torpedo-like manner allows a precise realization of the given control task with fewer control signals, comparing to the ones using a unicycle-like strategy.

In this paper, we focus on the development of the control structure guaranteeing a realization of the path following motion task in the torpedo-like strategy by a spatially moving vehicle. In this research, the path is defined as a cross-section of two surfaces described by non-parametrized equations [20, 33, 44, 29]. On the contrary to the classical, parametrized way of defining the reference path [32, 11, 45], the utilized approach does not impose restrictive constraints on the initial conditions and does not demand a calculation of the shortest distance between a vehicle body and the path. The analytical calculation of the aforementioned path-to-vehicle distance, although straightforward in the case of simple examples (e.g. linear or circular paths), is in general non-trivial for more complex paths with a varying curvature and may be hard to obtain numerically in each control sample with a satisfying control-loop frequency.

The cascaded control structure presented in this article con-

*Corresponding author

Email addresses:

krzysztof.pi.lakomy@doctorate.put.poznan.pl (Krzysztof Łakomy*), maciej.michalek@put.poznan.pl (Maciej Marcin Michałek)

sists of the inner dynamic-level controller responsible for tracking of the commanded velocities, calculated by the outer kinematic-level controller in a way to attract the vehicle towards the reference path with a prescribed orientation. The dynamic-level control loop is designed according to the Active Disturbance Rejection (ADR) method [12, 9, 42, 4] introducing a feedforward control from a total disturbance. The effort made to compensate the total disturbance makes the presented control algorithm robust to external forces (caused by winds, currents, etc.) and to parametric uncertainties of a vehicle mathematical model. Due to the use of an error-domain Extended State Observer (ESO) [25, 23], being a part of the ADR controller, the whole control structure has got output-feedback characteristics, which means that it only needs to measure the vehicle position and attitude to achieve expected control quality. The output-feedback property is practically desirable, because measuring all of the state vector elements, including longitudinal velocities, may be expensive (when measured by high-quality sensors) or computationally challenging when estimated upon the visual data. The outer kinematic-level controller uses the Vector Field Orientation (VFO) methodology, introduced initially for wheeled robots in [27], and developed recently for the 3D vehicle motion [28, 20]. The kinematic controller aims to calculate a vector of commanded velocities, which, while being correctly followed by a dynamic controller, guarantee an accurate following of the reference path.

This paper is a substantial extension of the conference articles [20] and [21], providing a more detailed description and a formal analysis of the VFO-ADR control structure satisfying the non-parametrized path-following in a torpedo-like motion strategy of the vehicle moving in a 3D space. Comparing to the results presented in [20], the VFO controller is extended by the transversal drift compensation component, causing a significant increase in the path-following control performance for the case of underactuated vehicles. Unlike the most common cascade control systems designed for the UAV/AUV-type objects, that are based on the decoupling of the longitudinal and angular subsystems, we propose to use the approach utilized in the control of nonholonomic vehicles that decouples system kinematics from system dynamics (see also [40]). Many solutions considering the ADR-based control of the spatial mobile vehicles, for example [4, 46], demand the measurements of the whole state vector. On the contrary to these methods, the ADR controller presented in this article uses the error-domain architecture of ESO and only needs the information about the system configuration. The use of the ADR method in the inner-loop controller guarantees also the robustness of the proposed control structure to the external disturbances and significant model uncertainties. According to the Input-to-State Stability (ISS) procedure [18, 36] conducted in the multi-input approach [15, 30], application of the VFO-ADR control structure to the dynamics of the considered vehicle results in the bounded control errors and a possible reduction of positional errors to arbitrarily small magnitudes. The theoretical analysis is followed by the simulation verification performed in the Matlab/Simulink environment.

Notation. For the sake of the notational conciseness, we will use the assignments $s\alpha \equiv \sin\alpha$, $c\alpha \equiv \cos\alpha$, $t\alpha \equiv \tan\alpha$, and

$l s_\infty := \limsup_{t \rightarrow \infty}$. The nabla operator was treated as a column vector $\nabla = [\partial/\partial x \ \partial/\partial y \ \partial/\partial z]^\top$ and the set $\mathbb{R}_{\geq 0} = \{x \in \mathbb{R} : x \geq 0\}$. In order not to make the equations excessively long, we have omitted the signal parameters in longer formulas.

2. Preliminaries

2.1. Mathematical model of a vehicle

To describe the position and attitude of a rigid-body vehicle in a 3D space, the global frame $\{G\}$ and the local (body-fixed) frame $\{B\}$ need to be introduced. The origin of $\{B\}$ is placed in the robot mass center C , while the x^B axis is aligned with the direction of the main thrust provided by the onboard actuation system. The configuration vector is represented as

$$\boldsymbol{\eta} = \begin{bmatrix} \boldsymbol{\eta}_p \\ \boldsymbol{\eta}_o \end{bmatrix} \triangleq \begin{bmatrix} [x \ y \ z]^\top \\ [\phi \ \theta \ \psi]^\top \end{bmatrix} \in \mathbb{R}^3 \times [-\pi, \pi) \times \left(-\frac{\pi}{2}, \frac{\pi}{2}\right) \times \mathbb{R}, \quad (1)$$

where $\boldsymbol{\eta}_p \triangleq [x \ y \ z]^\top$ describes the position of the $\{B\}$ origin in a global frame, while $\boldsymbol{\eta}_o \triangleq [\phi \ \theta \ \psi]^\top$ is a vector of RPY (Roll, Pitch, Yaw) Euler angles describing the vehicle attitude. The vector of pseudovelocities in the local frame

$$\boldsymbol{v} = \begin{bmatrix} \boldsymbol{v}_p \\ \boldsymbol{v}_o \end{bmatrix} \triangleq \begin{bmatrix} [u \ v \ w]^\top \\ [p \ q \ r]^\top \end{bmatrix} \in \mathbb{R}^6 \quad (2)$$

consists of the subvector of longitudinal velocities $\boldsymbol{v}_p \triangleq [u \ v \ w]^\top$ and the subvector of angular velocities $\boldsymbol{v}_o \triangleq [p \ q \ r]^\top$. The graphical representation of the 3D rigid body, together with the axes of $\{G\}$ and $\{B\}$, chosen elements of the configuration vector (1) and the vector of the pseudovelocities (2) is illustrated in Fig. 1.

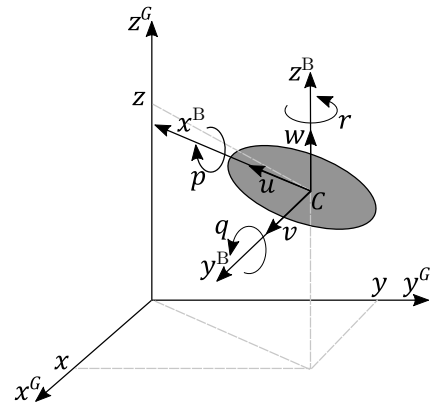


Figure 1: A rigid body in the 3D space.

Kinematics of the considered rigid vehicle, i.e., the velocity transformation between the local and global frames is expressed by

$$\dot{\boldsymbol{\eta}} = \boldsymbol{J}(\boldsymbol{\eta}_o)\boldsymbol{v}, \quad (3)$$

where $\boldsymbol{J}(\boldsymbol{\eta}_o) = \text{blkdiag}\{\boldsymbol{R}(\boldsymbol{\eta}_o), \boldsymbol{T}(\boldsymbol{\eta}_o)\}$ is the Jacobian matrix dependent on the rotation matrix $\boldsymbol{R}(\boldsymbol{\eta}_o)$ and the angular velocity

transformation matrix $T(\eta_o)$ that are, respectively, defined as

$$\mathbf{R}(\eta_o) = \begin{bmatrix} c\psi c\theta & c\psi s\phi s\theta - c\phi s\psi & c\psi c\phi s\theta + s\phi s\psi \\ s\psi c\theta & s\psi s\phi s\theta + c\phi c\psi & s\psi c\phi s\theta - s\phi c\psi \\ -s\theta & s\phi c\theta & c\phi c\theta \end{bmatrix}, \quad (4)$$

$$\mathbf{T}(\eta_o) = \begin{bmatrix} 1 & s\phi t\theta & c\phi t\theta \\ 0 & c\phi & -s\phi \\ 0 & s\phi/c\theta & c\phi/c\theta \end{bmatrix}. \quad (5)$$

Remark 1. To prevent the vehicle configuration running into the singular points of transformation $\mathbf{T}(\eta_o)$, the pitch angle is restricted in the sense that $\forall_{t \geq 0} \theta(t) \in \left(-\frac{\pi}{2}, \frac{\pi}{2}\right)$, see (1).

According to the work [8], general equations of the 6 DoF rigid body dynamics are respectively expressed in the global and local frames as

$$\{G\}: \mathbf{M}_\eta(\eta)\ddot{\eta} + \boldsymbol{\mu}_\eta(\eta, \dot{\eta}) + \boldsymbol{\tau}_\eta^* = \boldsymbol{\Gamma}_\eta(\eta)\boldsymbol{\tau}_\eta, \quad (6)$$

$$\{B\}: \mathbf{M}\dot{\mathbf{v}} + \boldsymbol{\mu}(\eta, \mathbf{v}) + \boldsymbol{\tau}^* = \boldsymbol{\Gamma}\boldsymbol{\tau}. \quad (7)$$

where \mathbf{M}_η , \mathbf{M} are the inertia matrices, $\boldsymbol{\mu}_\eta$, $\boldsymbol{\mu}$ represent the vectors accumulating the gravitational, Coriolis, centripetal and restoring forces together with the influence of environmental damping terms, $\boldsymbol{\tau}_\eta$, $\boldsymbol{\tau}$ are the control signal vectors (corresponding to the forces and torques along/around particular axes), while $\boldsymbol{\tau}_\eta^*$, $\boldsymbol{\tau}^*$ refer to the combined external disturbances and the unmodeled dynamic phenomena. Relations between the matrices and vectors occurring in the equations of robot dynamics (6)-(7) are as follows: $\mathbf{M} = \mathbf{J}^\top \mathbf{M}_\eta \mathbf{J}$, $\boldsymbol{\mu} = \mathbf{J}^\top (\boldsymbol{\mu}_\eta + \mathbf{M}_\eta \mathbf{J} \mathbf{v})$, $\boldsymbol{\tau}^* = \mathbf{J}^\top \boldsymbol{\tau}_\eta^*$ and $\boldsymbol{\tau} = \mathbf{J}^\top \boldsymbol{\tau}_\eta$. Input matrices

$$\boldsymbol{\Gamma} \triangleq \text{diag}\{1, \gamma_v, \gamma_w, \gamma_p, 1, 1\}, \quad \gamma_v, \gamma_w \in \{0, 1\} \quad (8)$$

and $\boldsymbol{\Gamma}_\eta = \mathbf{J}^{-\top} \boldsymbol{\Gamma} \mathbf{J}^\top$ determine the type of an actuation system mounted on the vehicle in such a manner, that for $\gamma_i = 0$ and $i \in \{v, w, p\}$, the control signal in a particular axis cannot be generated, causing the non-actuation of the corresponding DoF. A selected form of the matrix $\boldsymbol{\Gamma}$ implies that the surge, pitch, and yaw axes are certainly actuated, and thus the privileged direction of motion should be described along with them. Within this research, we assume the anisotropy of the robot actuation system (see [28]) even in the fully actuated case, implying that even if the forces along y^B , z^B , and around x^B axes can be generated, they only fulfill the compensation function due to the lower capabilities of the thrust-generating actuators in these directions. The aforementioned actuator distribution justifies the selection of a torpedo-like motion strategy described in the Introduction (see also [28, 14]).

The overall state-space equations of the considered rigid body vehicle (assuming the invertability of \mathbf{M} , see [8]) are represented by a set of differential equations

$$\begin{cases} \dot{\eta} = \mathbf{J}(\eta_o)\mathbf{v}, \\ \dot{\mathbf{v}} = -\mathbf{M}^{-1}[\boldsymbol{\mu}(\eta, \mathbf{v}) + \boldsymbol{\tau}^*] + \mathbf{M}^{-1}\boldsymbol{\Gamma}\boldsymbol{\tau}. \end{cases} \quad (9)$$

The dynamical system (9) will be further considered under following assumptions:

Assumption 1. Configuration vector $\boldsymbol{\eta}(t)$ is the only measurable signal that can be used to design a control law.

Assumption 2. The vehicle dynamics (9) is structurally and parametrically uncertain.

Assumption 3. The elements of vector $\boldsymbol{\tau}^*(t)$ are bounded Lipschitz functions.

Assumption 4. We analyze a subclass of systems described by (9), restricted to the objects where the roll axis is actuated, implying that $\gamma_p = 1$, see (8).

2.2. Reference path definition

According to the definition introduced in [20] and [33], the positional reference path can be considered as a set of reference points

$$\mathcal{S}_d \triangleq \{\boldsymbol{\eta}_p = \boldsymbol{\eta}_{pd} = [x_d \ y_d \ z_d]^\top \in \mathcal{D} : s_1(\boldsymbol{\eta}_{pd}) = s_2(\boldsymbol{\eta}_{pd}) = 0\}, \quad (10)$$

where \mathcal{D} is a domain of admissible robot positions. Set \mathcal{S}_d is interpreted as a cross-section of the surfaces described with a pair of the non-parametric functions $s_1(\boldsymbol{\eta}_p)$ and $s_2(\boldsymbol{\eta}_p)$. Besides the geometrical curve definition itself, we define the reference velocity along the path

$$u_d \triangleq \xi_d U, \quad U = \text{const} > 0, \quad \xi_d \in \{-1, +1\}, \quad (11)$$

where ξ_d determines the movement strategy ($\xi_d = -1$ for backward and $\xi_d = +1$ for forward movement). Due to a non-zero value of the constant U , the velocity u_d impose a persistently exciting reference motion for a vehicle.

Remark 2. The velocity u_d introduced in (11) is assumed to be constant for the sake of simplicity. In more general case, it can depend on the position $\boldsymbol{\eta}_p$.

Consistently with [20], let us introduce some assumptions concerning surfaces $s_1(\boldsymbol{\eta}_p)$ and $s_2(\boldsymbol{\eta}_p)$, which will be necessary for the control design purposes.

Assumption 5. For all admissible points $\boldsymbol{\eta}_p \in \mathcal{D}$, the gradient of the j -th level-surface, i.e., $\nabla s_j(\boldsymbol{\eta}_p) \triangleq [\partial s_j / \partial x \ \partial s_j / \partial y \ \partial s_j / \partial z]^\top$ has a finite, and strictly positive norm: $\forall \boldsymbol{\eta}_p \in \mathcal{D}$, $\underline{m}_j < \|\nabla s_j(\boldsymbol{\eta}_p)\| < \bar{m}_j$, for $\underline{m}_j, \bar{m}_j > 0$ and $j \in \{1, 2\}$.

Assumption 6. For all admissible points $\boldsymbol{\eta}_p \in \mathcal{D}$, the derivatives of the j -th level-surface with respect to the arguments up to the order 3 are bounded, and the Hessian $\nabla(\nabla^\top s_j(\boldsymbol{\eta}_p)) \in \mathbb{R}^{3 \times 3}$ has a finite norm, that is, $\forall \boldsymbol{\eta}_p \in \mathcal{D}$, $\|\nabla(\nabla^\top s_j(\boldsymbol{\eta}_p))\| < \bar{M}_j$, for $\bar{M}_j > 0$ and $j \in \{1, 2\}$.

Assumption 7. For all admissible positions $\boldsymbol{\eta}_p \in \mathcal{D}$, gradients of functions $s_1(\boldsymbol{\eta}_p)$, $s_2(\boldsymbol{\eta}_p)$ are not collinear: $\forall \boldsymbol{\eta}_p \in \mathcal{D} \ \nabla s_1(\boldsymbol{\eta}_p) \neq k \nabla s_2(\boldsymbol{\eta}_p)$, $k \in \mathbb{R}$.

To define the reference pitch and yaw angles along the path, we have to introduce unit vectors normal to the particular path-describing surfaces in the form

$$\boldsymbol{\vartheta}_j(\boldsymbol{\eta}_p) = \begin{bmatrix} \vartheta_{jx}(\boldsymbol{\eta}_p) \\ \vartheta_{jy}(\boldsymbol{\eta}_p) \\ \vartheta_{jz}(\boldsymbol{\eta}_p) \end{bmatrix} \triangleq -\frac{\nabla s_j(\boldsymbol{\eta}_p)}{\|\nabla s_j(\boldsymbol{\eta}_p)\|}, \text{ for } j \in \{1, 2\}, \quad (12)$$

and a unit vector tangential to both surfaces represented by

$$\boldsymbol{\vartheta}_\perp(\boldsymbol{\eta}_p) = \begin{bmatrix} \vartheta_{\perp x}(\boldsymbol{\eta}_p) \\ \vartheta_{\perp y}(\boldsymbol{\eta}_p) \\ \vartheta_{\perp z}(\boldsymbol{\eta}_p) \end{bmatrix} \triangleq \sigma \left[\boldsymbol{\vartheta}_1(\boldsymbol{\eta}_p) \times \boldsymbol{\vartheta}_2(\boldsymbol{\eta}_p) \right], \quad (13)$$

where $\sigma \in \{-1, 1\}$ describes the desired movement direction along the path. In the case when the vehicle position $\boldsymbol{\eta}_p \notin \mathcal{S}_d$, the values of $s_1(\boldsymbol{\eta}_p)$, $s_2(\boldsymbol{\eta}_p)$ are not zero, and $\boldsymbol{\vartheta}_\perp(\boldsymbol{\eta}_p)$ is not necessarily aligned with the reference path. Surface $s_j(\boldsymbol{\eta}_p) = k$, $k \in \mathbb{R}$ will henceforth be called a *level-surface* on the level k .

Remark 3. To avoid the situation, when the reference motion goes through the singularity point described in the Remark 1, the level-surface equations should be designed in a way to guarantee

$$m_\perp < \|\bar{\boldsymbol{\vartheta}}_\perp(\boldsymbol{\eta}_{pd})\|, \quad m_\perp > 0, \quad (14)$$

for $\bar{\boldsymbol{\vartheta}}_\perp(\boldsymbol{\eta}_{pd}) \triangleq [\vartheta_{\perp x} \ \vartheta_{\perp y}]^\top$ being a projection of $\boldsymbol{\vartheta}_\perp(\boldsymbol{\eta}_{pd})$ onto the $x^G y^G$ plane.

Due to the underactuation of the considered vehicle along the y^B , z^B , and around x^B axes, see (8), and the fact that the main propulsion is acting in the surge direction, the reference attitude of the x^B axis should be aligned with the reference path, implying the reference yaw, pitch, and roll angles to be defined, respectively, as

$$\psi_d(\boldsymbol{\eta}_{pd}) \triangleq \text{Atan2}(\xi_d \vartheta_{\perp y}(\boldsymbol{\eta}_{pd}), \xi_d \vartheta_{\perp x}(\boldsymbol{\eta}_{pd})) \in [-\pi, \pi), \quad (15)$$

$$\theta_d(\boldsymbol{\eta}_{pd}) \triangleq \arctan(-\vartheta_{\perp z}(\boldsymbol{\eta}_{pd})/\beta_1(\boldsymbol{\eta}_{pd})) \in \left(-\frac{\pi}{2}, \frac{\pi}{2}\right), \quad (16)$$

$$\phi_d(\boldsymbol{\eta}_{pd}) \triangleq 0, \quad (17)$$

where $\text{Atan2} : \mathbb{R} \times \mathbb{R} \rightarrow [-\pi, \pi)$ is a four-quadrant inverse tangent function including the bi-valued variable ξ_d introduced in (11), while

$$\beta_1(\boldsymbol{\eta}_{pd}) = \vartheta_{\perp x}(\boldsymbol{\eta}_{pd})c\psi_d(\boldsymbol{\eta}_{pd}) + \vartheta_{\perp y}(\boldsymbol{\eta}_{pd})s\psi_d(\boldsymbol{\eta}_{pd}). \quad (18)$$

Remark 4. The motion strategy considered within this article is assumed to have a non-banked characteristic (see [8]), implying the y^B axis to be parallel to the $x^G y^G$ plane, and resulting in the fixed value of the reference roll angle $\phi_d \equiv 0$ introduced in (17).

2.3. Formulation of control objectives

Let the path-following errors be accumulated in the vector

$$\boldsymbol{\epsilon}(\boldsymbol{\eta}) = \begin{bmatrix} \boldsymbol{e}_p(\boldsymbol{\eta}_p) \\ \boldsymbol{e}_o(\boldsymbol{\eta}) \end{bmatrix} \triangleq \begin{bmatrix} s_1(\boldsymbol{\eta}_p) \\ s_2(\boldsymbol{\eta}_p) \\ \phi_d - \phi \\ \theta_d(\boldsymbol{\eta}_p) - \theta \\ \psi_d(\boldsymbol{\eta}_p) - \psi \end{bmatrix} \in \mathcal{Q}_e, \quad (19)$$

where $\mathcal{Q}_e = \mathbb{R}^2 \times [-\pi, \pi)^2 \times \mathbb{R}$. The values of each level-surface, $s_1(\boldsymbol{\eta}_p)$ or $s_2(\boldsymbol{\eta}_p)$, correspond to some non-Euclidean measure of the signed distance between the origin of $\{B\}$ and the particular level-surface. The control objective of the path-following task is to find an output-feedback control law $\boldsymbol{\tau} = \boldsymbol{\tau}(\boldsymbol{\eta})$ that when applied into (9), guarantees the boundedness of the error

$$\boldsymbol{e}_{2\pi}(\boldsymbol{\eta}) \triangleq \begin{bmatrix} \boldsymbol{e}_p(\boldsymbol{\eta}_p) \\ \boldsymbol{e}_o(\boldsymbol{\eta}) \bmod 2\pi \end{bmatrix} \quad (20)$$

in the sense that

$$\exists T \in [0, \infty) : \forall t \geq T \ \|\boldsymbol{e}_{2\pi}(\boldsymbol{\eta}(t))\| \leq \varepsilon_\eta, \quad (21)$$

$$\exists T \in [0, \infty) : \forall t \geq T \ \|\boldsymbol{e}_p(\boldsymbol{\eta}_p(t))\| \leq \varepsilon_p, \quad (22)$$

for some upper bounds $\varepsilon_\eta, \varepsilon_p > 0$, where ε_p can be made arbitrarily small. The modulo 2π operation utilized in (20) on the angular error vector $\boldsymbol{e}_o(\boldsymbol{\eta})$ is introduced to limit the domain of yaw angle error $e_\psi \triangleq \psi_d - \psi \in \mathbb{R}$ introduced in (19).

3. The design of VFO-ADR controller

The kinematic-level VFO controller presented in this article uses the values of the velocity error estimates calculated by ESO. As a consequence, we will start with the presentation of the dynamic-level ADR controller explaining the procedure of estimating required signals, and continue with the description of the VFO path-following controller.

3.1. Dynamic-level ADR controller

The main task of the inner dynamic-level controller is to calculate the values of the generalized forces applied to the vehicle body, aggregated within the control signal vector $\boldsymbol{\tau}$ introduced in the equation (7). Obtained values of the control signals should guarantee tracking of the commanded velocities

$$\dot{\boldsymbol{\eta}}_c(t) = \begin{bmatrix} \dot{\boldsymbol{\eta}}_{pc}(t) \\ \dot{\boldsymbol{\eta}}_{oc}(t) \end{bmatrix} = \boldsymbol{J}(\boldsymbol{\eta}_o(t))\boldsymbol{v}_c(t), \quad (23)$$

with sufficient accuracy. The vector of commanded velocities $\dot{\boldsymbol{\eta}}_c(t)$ expressed in the global frame $\{G\}$ is calculated using the Jacobian matrix introduced in (3) and the commanded pseudovelocity vector

$$\boldsymbol{v}_c = \begin{bmatrix} \boldsymbol{v}_{pc} \\ \boldsymbol{v}_{oc} \end{bmatrix} \triangleq \begin{bmatrix} [u_c \ v_c \ w_c]^\top \\ [p_c \ q_c \ r_c]^\top \end{bmatrix} \in \mathbb{R}^6 \quad (24)$$

expressed in the body-fixed frame. Vector \boldsymbol{v}_c is computed online by the VFO kinematic (outer-loop) controller described in Section 3.2.

The velocity tracking error in the global coordinate system is defined as

$$\boldsymbol{\epsilon}(t) \triangleq \dot{\boldsymbol{\eta}}_c(t) - \dot{\boldsymbol{\eta}}(t) = \begin{bmatrix} \boldsymbol{\epsilon}_p(t) \\ \boldsymbol{\epsilon}_o(t) \end{bmatrix} = \begin{bmatrix} [\epsilon_1(t) \ \epsilon_2(t) \ \epsilon_3(t)]^\top \\ [\epsilon_4(t) \ \epsilon_5(t) \ \epsilon_6(t)]^\top \end{bmatrix}, \quad (25)$$

while its dynamics can be derived upon (6) and (7) in the form

$$\begin{aligned}
\dot{\epsilon} &= \dot{\eta}_c - \dot{\eta} = \ddot{\eta}_c + \mathbf{M}_\eta^{-1} [\boldsymbol{\mu}_\eta + \boldsymbol{\tau}_\eta^*] \\
&\quad - \mathbf{M}_\eta^{-1} \boldsymbol{\Gamma}_\eta \boldsymbol{\tau}_\eta + \hat{\mathbf{B}}_\eta \boldsymbol{\Gamma}_\eta \boldsymbol{\tau}_\eta - \hat{\mathbf{B}}_\eta \boldsymbol{\Gamma}_\eta \boldsymbol{\tau}_\eta \\
&= \mathbf{d}(\dot{\eta}_c, \boldsymbol{\eta}, \dot{\boldsymbol{\eta}}, \boldsymbol{\tau}_\eta, \boldsymbol{\tau}_\eta^*) - \hat{\mathbf{B}}_\eta \boldsymbol{\Gamma}_\eta \boldsymbol{\tau}_\eta \\
&= \mathbf{d}(\dot{\eta}_c, \boldsymbol{\eta}, \dot{\boldsymbol{\eta}}, \boldsymbol{\tau}_\eta, \boldsymbol{\tau}_\eta^*) - \mathbf{J} \hat{\mathbf{B}} \boldsymbol{\Gamma} \mathbf{J}^\top \boldsymbol{\tau}_\eta. \tag{26}
\end{aligned}$$

Referring to the commonly used nomenclature utilized in the ADR-focused research (e.g. [12, 42]), vector $\mathbf{d}(\cdot) \triangleq [d_1(\cdot) \dots d_6(\cdot)]^\top$ will be treated as the so-called *total disturbance* of system (26), while $\hat{\mathbf{B}}_\eta \in \mathbb{R}^{6 \times 6}$, and $\hat{\mathbf{B}} \triangleq \text{diag}\{\hat{b}_1, \dots, \hat{b}_6\} \in \mathbb{R}^{6 \times 6}$ are, respectively, the rough approximations of the \mathbf{M}_η^{-1} and \mathbf{M}^{-1} matrices. The mutual relation between the the inverse inertia matrices in global, and body-fixed coordinate frames has the form $\mathbf{M}_\eta^{-1} = \mathbf{J} \mathbf{M}^{-1} \mathbf{J}^\top$, thus, the corresponding relation between their estimates can be written down as $\hat{\mathbf{B}}_\eta = \mathbf{J} \hat{\mathbf{B}} \mathbf{J}^\top$.

A specific representation of the input signals influencing the dynamical system represented by (6) and (7) results in the possibility of designing the controls $\boldsymbol{\tau}$, $\boldsymbol{\tau}_\eta$ in the same way for the underactuated vehicle as for the fully-actuated one. Particular elements of the control vectors, associated with the non-actuated axes, will be later cut out by the matrices $\boldsymbol{\Gamma}$, $\boldsymbol{\Gamma}_\eta$ implying the applied control vectors to be in the form $\boldsymbol{\Gamma} \boldsymbol{\tau}$, $\boldsymbol{\Gamma}_\eta \boldsymbol{\tau}_\eta$ for the $\{B\}$ and $\{G\}$ frames, respectively.

Remark 5. *A lack of control signals in the non-actuated axes results in the presence of a transversal drift affecting the system dynamic behavior and lowering the path-following precision. This phenomenon can be suppressed with a properly designed kinematic-level controller compensating the transversal-drift.*

According to the velocity error dynamics derived in (26), we propose the following nominal control law for generalized forces

$$\begin{aligned}
\boldsymbol{\tau}_\eta &\triangleq \hat{\mathbf{B}}_\eta^{-1} [\hat{\mathbf{d}} + \mathbf{K}_\eta \hat{\epsilon}] \\
&= \mathbf{J}^{-\top} \hat{\mathbf{B}}^{-1} \mathbf{J}^{-1} [\hat{\mathbf{d}} + \mathbf{K}_\eta \hat{\epsilon}], \tag{27}
\end{aligned}$$

where $\hat{\mathbf{d}}$ is an estimated value of the total disturbance, $\hat{\epsilon}$ is an estimate of velocity tracking error, and $\mathbf{K}_\eta \in \mathbb{R}^{6 \times 6}$ denotes the gain matrix of the ADR controller.

Remark 6. *According to Assumption 1, $\boldsymbol{\eta}$ is the only measurable signal that we can use in the design of feedback control. Vectors \mathbf{d} and $\boldsymbol{\epsilon}$ are dependent not only on the configuration vector, but also on its derivative, therefore in (27) we utilized the estimates $\hat{\mathbf{d}}$ and $\hat{\epsilon}$ which will be calculated by the extended state observer presented in the latter part of this subsection.*

According to the mutual relations of the particular model components presented in the description of (6) and (7), we can transform the control signals represented in frame $\{G\}$ to the local coordinate system $\{B\}$ expressing them as

$$\begin{aligned}
\boldsymbol{\tau} &= \mathbf{J}^\top \boldsymbol{\tau}_\eta \stackrel{(27)}{=} \hat{\mathbf{B}}^{-1} \mathbf{J}^{-1} [\hat{\mathbf{d}} + \mathbf{K}_\eta \hat{\epsilon}] \\
&= [\tau_u \ \tau_v \ \tau_w \ \tau_p \ \tau_q \ \tau_r]^\top. \tag{28}
\end{aligned}$$

We propose to obtain the estimates $\hat{\boldsymbol{\epsilon}}$ and $\hat{\mathbf{d}}$, utilized in (27) and (28), using the high-gain linear ESO (see [28, 19]). The vector of an extended state associated with the particular degree of freedom can be defined as

$$\mathbf{x}_i = \begin{bmatrix} x_{1i} \\ x_{2i} \\ x_{3i} \end{bmatrix} \triangleq \begin{bmatrix} \eta_{ci} - \eta_i \\ \epsilon_i \\ d_i \end{bmatrix} \in \mathbb{R}^3, \quad i \in \{1, \dots, 6\}, \tag{29}$$

where $\boldsymbol{\eta}_c(t) = [\eta_{c1}(t) \dots \eta_{c6}(t)]^\top \triangleq \boldsymbol{\eta}(0) + \int_0^t \mathbf{J}(\boldsymbol{\eta}_o(\xi)) \mathbf{v}_c(\xi) d\xi$ and η_i corresponds to the i -th element of the configuration vector (1). The state-space equations of the i -th extended state vector dynamics, calculated upon (26), are expressed by

$$\begin{cases} \dot{\mathbf{x}}_i = \underbrace{\begin{bmatrix} 0 & 1 & 0 \\ 0 & 0 & 1 \\ 0 & 0 & 0 \end{bmatrix}}_A \mathbf{x}_i + \underbrace{\begin{bmatrix} 0 \\ -1 \\ 0 \end{bmatrix}}_b \zeta_i^\top \mathbf{J} \hat{\mathbf{B}} \boldsymbol{\Gamma} \mathbf{J}^\top \boldsymbol{\tau}_\eta + \begin{bmatrix} 0 \\ 0 \\ 1 \end{bmatrix} \dot{d}_i \\ y_i = \begin{bmatrix} 1 & 0 & 0 \end{bmatrix} \mathbf{x}_i = \mathbf{C} \mathbf{x}_i, \end{cases} \tag{30}$$

where

$$\zeta_i^\top = [\zeta_{i1} \dots \zeta_{i6}] \in \mathbb{R}^6 : \zeta_{ij} \triangleq \begin{cases} 1, & \text{when } i = j \\ 0, & \text{when } i \neq j \end{cases} \tag{31}$$

is a cutting out vector, selecting the appropriate element of the control input vector.

According to equation (30), we propose a linear observer for a single degree of freedom

$$\dot{\hat{\mathbf{x}}}_i = \mathbf{A} \hat{\mathbf{x}}_i + \mathbf{b} \zeta_i^\top \mathbf{J} \hat{\mathbf{B}} \boldsymbol{\Gamma} \mathbf{J}^\top \boldsymbol{\tau}_\eta + l_i [(\eta_{ci} - \eta_i) - \hat{x}_{1i}], \tag{32}$$

where $\hat{\mathbf{x}}_i \triangleq [\hat{x}_{1i} \ \hat{x}_{2i} \ \hat{x}_{3i}]^\top$ is an estimate of the extended state vector (29), while

$$\mathbf{l}_i = [l_{1i} \ l_{2i} \ l_{3i}]^\top \triangleq [3\omega_{oi} \ 3\omega_{oi}^2 \ \omega_{oi}^3]^\top, \quad \omega_{oi} > 0 \tag{33}$$

is a vector of observer gains. Tuning strategy of the observer gains expressed by (33) is based on the choice of a single parameter value (ω_{oi}), interpreted as a bandwidth pulsation of ESO (see [9]).

3.2. Kinematic-level VFO controller

The outer-loop controller is designed according to the VFO methodology [27, 28] and results in the calculation of the commanded velocity vector \mathbf{v}_c , see (24), satisfying the desired torpedo-like motion strategy along the reference path. For the design purposes, we are going to keep

$$\phi(t) = 0, \tag{34}$$

according to the postulated non-banked motion (see Remark 4). As a consequence, the roll angle error introduced in (19) should satisfy $\forall t \geq 0 \ e_\phi(t) = \phi_d(t) - \phi(t) = 0$. Stabilization of the roll angle is obtained with the use of an auxiliary controller designed according to the vehicle kinematics (3) as

$$p_c(t) \triangleq f_\phi(e_\phi(t), \cdot) - s\phi(t)t\theta(t) q_c(t) - c\phi(t)t\theta(t) r_c(t), \tag{35}$$

where $f_\phi(e_\phi(t), \cdot)$ is a feedback function that should guarantee the error $e_\phi(t)$ to converge to zero. At this step, we are not choosing any particular function $f_\phi(e_\phi, \cdot)$ - we will introduce and discuss one in the section considering the simulation/experimental results of the proposed control structure.

Assumption 8. According to a fixed value of the desired roll angle (17) and a proper selection of the $f_\phi(e_\phi, \cdot)$ function, we assume that the controlled object fulfills the non-banked motion strategy, satisfying

$$\forall t > T, \phi(t) = 0 \quad (36)$$

for some finite time T .

According to the torpedo-like motion philosophy, the components of the commanded velocity vector v_c associated with the non-privileged longitudinal axes are fixed at the zero values, i.e., $v_c \triangleq 0$ and $w_c \triangleq 0$, implying that the velocities

$$v(t) = \epsilon_v(t), \quad w(t) = \epsilon_w(t), \quad (37)$$

where $\epsilon_v(t)$ and $\epsilon_w(t)$ are the elements of the velocity tracking error vector in the body-fixed frame as

$$\begin{aligned} \epsilon_v &= [\epsilon_u \ \epsilon_v \ \epsilon_w \ \epsilon_p \ \epsilon_q \ \epsilon_r]^\top \\ &\triangleq v_c - v = J^{-1}(\eta_o)\dot{\eta}_c - J^{-1}(\eta_o)\dot{\eta} = J^{-1}(\eta_o)\epsilon. \end{aligned} \quad (38)$$

Application of the VFO controller proposed in [20] to the underactuated vehicle will not provide a satisfactory control performance (especially in the not actuated degrees of freedom), thus we propose a modification of the kinematic-level controller to deal with the transversal-drift appearing in the non-actuated axes. The VFO kinematic control law will be derived assuming that the postulate (36) is satisfied and for the equations (37). Upon the definition (25) and the design assumption (34), vehicle kinematics (3) can be rewritten in a simplified form

$$\begin{aligned} \begin{bmatrix} \dot{x} \\ \dot{y} \\ \dot{z} \\ \dot{\theta} \\ \dot{\psi} \end{bmatrix} &= \begin{bmatrix} c\psi c\theta & 0 & 0 \\ s\psi c\theta & 0 & 0 \\ -s\theta & 0 & 0 \\ 0 & 1 & 0 \\ 0 & 0 & \frac{1}{c\theta} \end{bmatrix} \begin{bmatrix} u_c \\ q_c \\ r_c \end{bmatrix} - \begin{bmatrix} \epsilon_1 \\ \epsilon_2 \\ \epsilon_3 \\ \epsilon_5 \\ \epsilon_6 \end{bmatrix} \\ &\Leftarrow \dot{\eta} = G(\bar{\eta})\bar{v}_c - \bar{\epsilon}, \end{aligned} \quad (39)$$

where $\bar{\eta} = [x \ y \ z \ \theta \ \psi]^\top \in \mathbb{R}^5$, $\bar{v}_c = [u_c \ q_c \ r_c]^\top \in \mathbb{R}^3$, and $\bar{\epsilon} = [\epsilon_1 \ \epsilon_2 \ \epsilon_3 \ \epsilon_5 \ \epsilon_6]^\top \in \mathbb{R}^5$ are reduced versions of the original vectors. According to the assumptions of the VFO methodology described in [27], the vehicle should move along the integral curves determined by the so-called *convergence vector field*, marked as

$$\begin{aligned} \mathbf{h}(\bar{\eta}, t) &= \begin{bmatrix} \mathbf{h}_p(\bar{\eta}, t) \\ \mathbf{h}_o(\bar{\eta}, t) \end{bmatrix} \in \mathbb{R}^5, \text{ where} \quad (40) \\ \mathbf{h}_p &= \begin{bmatrix} h_x \\ h_y \\ h_z \end{bmatrix} \in \mathbb{R}^3, \quad \mathbf{h}_o = \begin{bmatrix} h_\theta \\ h_\psi \end{bmatrix} \in \mathbb{R}^2. \end{aligned}$$

In the analyzed case, a properly designed vector field \mathbf{h} should guarantee that $\lim_{t \rightarrow \infty} [\mathbf{h}(t) - \bar{\eta}(t)] = 0$. According to the formula (39) and the form (40), the limit case can be rewritten as a postulate

$$\begin{bmatrix} h_x - u_c c\theta c\psi + \epsilon_1 \\ h_y - u_c c\theta s\psi + \epsilon_2 \\ h_z + u_c s\theta + \epsilon_3 \\ h_\theta - q_c + \epsilon_5 \\ h_\psi - \frac{1}{c\theta} r_c + \epsilon_6 \end{bmatrix} = \begin{bmatrix} 0 \\ 0 \\ 0 \\ 0 \\ 0 \end{bmatrix}. \quad (41)$$

Solving (41) with respect to \bar{v}_c , results in the nominal forms of pseudovelocities

$$\begin{aligned} \bar{v}_{cn} &= [u_{cn} \ q_{cn} \ r_{cn}]^\top \\ &\triangleq \begin{bmatrix} (h_x + \epsilon_1)c\theta c\psi + (h_y + \epsilon_2)c\theta s\psi - (h_z + \epsilon_3)s\theta \\ h_\theta + \epsilon_5 \\ (h_\psi + \epsilon_6)c\theta \end{bmatrix} \\ &= \begin{bmatrix} h_x^* c\theta c\psi + h_y^* c\theta s\psi - h_z^* s\theta \\ h_\theta^* \\ h_\psi^* c\theta \end{bmatrix}, \end{aligned} \quad (42)$$

where $\mathbf{h}^*(\mathbf{h}, \epsilon) = [\mathbf{h}_p^* \ \mathbf{h}_o^*]^\top = [h_x^* \ h_y^* \ h_z^* \ h_\theta^* \ h_\psi^*]^\top \triangleq \mathbf{h} + \bar{\epsilon}$ is a modified convergence vector field. The desired output-feedback characteristics of the final control structure implies the inability of taking velocity measurements and makes the direct use of the velocity tracking error ϵ in the controller equations impossible. To calculate the applied commanded velocities \bar{v}_c , we propose to utilize the modified convergence vector field

$$\hat{\mathbf{h}}^*(\mathbf{h}, \hat{\epsilon}) = \begin{bmatrix} \hat{\mathbf{h}}_p^*(\mathbf{h}_p, \hat{\epsilon}_p) \\ \hat{\mathbf{h}}_o^*(\mathbf{h}_o, \hat{\epsilon}_o) \end{bmatrix} \quad (43)$$

that takes the estimates of the velocity tracking error $\hat{\epsilon}$ in the place of unavailable vector ϵ . Let us first define the longitudinal part of the modified convergence vector field as

$$\hat{\mathbf{h}}_p^*(\mathbf{h}_p, \hat{\epsilon}_p) \triangleq \mathbf{h}_p + \delta_p \hat{\epsilon}_p, \quad (44)$$

where $\delta_p \in [0, 1]$ is the design parameter. According to the so-called *cautious compensation* method, utilized for the ground vehicles in [26], an introduction of δ_p will make the control algorithm more robust to the possible overcompensation of velocity tracking errors caused by a non-zero estimation errors of the extended states x_i .

To complete the definition of a modified convergence vector field from (44), we define the longitudinal part of the convergence vector field as follows

$$\mathbf{h}_p(\eta_p) \triangleq u_d \boldsymbol{\vartheta}_\perp(\eta_p) + k_p [s_1(\eta_p) \boldsymbol{\vartheta}_1(\eta_p) + s_2(\eta_p) \boldsymbol{\vartheta}_2(\eta_p)], \quad (45)$$

where $k_p > 0$ is a design parameter of the VFO kinematic controller, whereas unit vectors $\boldsymbol{\vartheta}_\perp$, $\boldsymbol{\vartheta}_j$ were defined in (13) and (12), respectively.

According to the equations (41) and (42), the postulated values of yaw and pitch angles should satisfy the so-called *orienting conditions* (see [28]):

$$\psi - \text{Atan2c}(\xi_d \hat{h}_y^*, \xi_d \hat{h}_x^*) = 0, \quad \text{and} \quad (46)$$

$$\theta - \arctan\left(\frac{-\hat{h}_z^*}{\hat{h}_x^* c\psi + \hat{h}_y^* s\psi}\right) = 0, \quad (47)$$

where $\text{Atan2c}(\cdot, \cdot) : \mathbb{R} \times \mathbb{R} \rightarrow \mathbb{R}$ is a continuous version of a four-quadrant function $\text{Atan2}(\cdot, \cdot) : \mathbb{R} \times \mathbb{R} \rightarrow [-\pi, \pi]$, and is described in detail in [27]. Referring to the vehicle kinematics (3), the dynamics of the Euler angles is described with a set of differential equations, making the instantaneous satisfaction of orienting conditions impossible. Due to this fact, we introduce an auxiliary angular error

$$\begin{aligned} \bar{e}_a(\boldsymbol{\eta}_p, \hat{\boldsymbol{\epsilon}}_p) &\triangleq \begin{bmatrix} e_{\theta_a}(\boldsymbol{\eta}_p, \hat{\boldsymbol{\epsilon}}_p) \\ e_{\psi_a}(\boldsymbol{\eta}_p, \hat{\boldsymbol{\epsilon}}_p) \end{bmatrix} \\ &\triangleq \begin{bmatrix} \theta_a(\boldsymbol{\eta}_p, \hat{\boldsymbol{\epsilon}}_p) - \theta \\ \psi_a(\boldsymbol{\eta}_p, \hat{\boldsymbol{\epsilon}}_p) - \psi \end{bmatrix} \in [-\pi, \pi) \times \mathbb{R}, \end{aligned} \quad (48)$$

where θ_a and ψ_a are the elements of the auxiliary orientation vector defined as

$$\begin{aligned} \bar{\boldsymbol{\eta}}_{oa}(\boldsymbol{\eta}_p, \hat{\boldsymbol{\epsilon}}_p) &= \begin{bmatrix} \theta_a(\boldsymbol{\eta}_p, \hat{\boldsymbol{\epsilon}}_p) \\ \psi_a(\boldsymbol{\eta}_p, \hat{\boldsymbol{\epsilon}}_p) \end{bmatrix} \\ &\triangleq \begin{bmatrix} \arctan\left(\frac{-\hat{h}_z^*(\boldsymbol{\eta}_p, \hat{\boldsymbol{\epsilon}}_p)}{\hat{h}_x^*(\boldsymbol{\eta}_p, \hat{\boldsymbol{\epsilon}}_p)c\psi_a + \hat{h}_y^*(\boldsymbol{\eta}_p, \hat{\boldsymbol{\epsilon}}_p)s\psi_a}\right) \\ \text{Atan2c}(\xi_d \hat{h}_y^*(\boldsymbol{\eta}_p, \hat{\boldsymbol{\epsilon}}_p), \xi_d \hat{h}_x^*(\boldsymbol{\eta}_p, \hat{\boldsymbol{\epsilon}}_p)) \end{bmatrix} \in \mathcal{Q}, \end{aligned} \quad (49)$$

for $\mathcal{Q} = (-\pi/2, \pi/2) \times \mathbb{R}$.

Remark 7. The auxiliary orientation vector defined by (49) expresses the orientation of a longitudinal part of modified convergence vector field $\hat{\boldsymbol{h}}_p^*$ defined by (44)-(45). When the vehicle is on a reference path and the velocity tracking error $\boldsymbol{\epsilon} = \mathbf{0}$ - the auxiliary orientation corresponds to the desired orientation determined by (15)-(16).

We propose the form of the angular convergence vector field introduced in (40) to be defined as

$$\boldsymbol{h}_o(\boldsymbol{\eta}, \boldsymbol{\epsilon}_p, \hat{\boldsymbol{\epsilon}}_p, \dot{\hat{\boldsymbol{\epsilon}}}_p) \triangleq \dot{\bar{\boldsymbol{\eta}}}_{oa}(\boldsymbol{\eta}, \boldsymbol{\epsilon}_p, \hat{\boldsymbol{\epsilon}}_p, \dot{\hat{\boldsymbol{\epsilon}}}_p) + \boldsymbol{K}_a \bar{\boldsymbol{e}}_a(\boldsymbol{\eta}_p, \hat{\boldsymbol{\epsilon}}_p), \quad (50)$$

where $\boldsymbol{K}_a = \text{diag}\{k_\theta, k_\psi\} : k_\theta, k_\psi > 0$ is a gain matrix, and $\dot{\bar{\boldsymbol{\eta}}}_{oa}(\cdot) = [\dot{\theta}_a(\cdot) \dot{\psi}_a(\cdot)]^\top$ results from the time-differentiation of (49), i.e.,

$$\dot{\psi}_a = \frac{\hat{h}_y^*(\boldsymbol{\eta}, \boldsymbol{\epsilon}_p, \hat{\boldsymbol{\epsilon}}_p)\hat{h}_x^*(\boldsymbol{\eta}_p, \hat{\boldsymbol{\epsilon}}_p) - \hat{h}_x^*(\boldsymbol{\eta}, \boldsymbol{\epsilon}_p, \hat{\boldsymbol{\epsilon}}_p)\hat{h}_y^*(\boldsymbol{\eta}_p, \hat{\boldsymbol{\epsilon}}_p)}{[\hat{h}_x^*(\boldsymbol{\eta}_p, \hat{\boldsymbol{\epsilon}}_p)]^2 + [\hat{h}_y^*(\boldsymbol{\eta}_p, \hat{\boldsymbol{\epsilon}}_p)]^2}, \quad (51)$$

$$\dot{\theta}_a = -\frac{\beta_2(\boldsymbol{\eta}, \boldsymbol{\epsilon}_p, \hat{\boldsymbol{\epsilon}}_p, \dot{\hat{\boldsymbol{\epsilon}}}_p)}{\beta_3(\boldsymbol{\eta}_p, \hat{\boldsymbol{\epsilon}}_p)}, \quad (52)$$

for

$$\begin{aligned} \beta_2(\boldsymbol{\eta}, \boldsymbol{\epsilon}_p, \hat{\boldsymbol{\epsilon}}_p, \dot{\hat{\boldsymbol{\epsilon}}}_p) &= \\ & \hat{h}_z^*(\boldsymbol{\eta}_p, \boldsymbol{\epsilon}_p, \hat{\boldsymbol{\epsilon}}_p)(\hat{h}_x^*(\boldsymbol{\eta}_p, \hat{\boldsymbol{\epsilon}}_p)c\psi_a + \hat{h}_y^*(\boldsymbol{\eta}_p, \hat{\boldsymbol{\epsilon}}_p)s\psi_a) \\ & - \hat{h}_z^*(\boldsymbol{\eta}_p, \hat{\boldsymbol{\epsilon}}_p)(\hat{h}_x^*(\boldsymbol{\eta}_p, \boldsymbol{\epsilon}_p, \hat{\boldsymbol{\epsilon}}_p)c\psi_a \\ & + \hat{h}_y^*(\boldsymbol{\eta}_p, \boldsymbol{\epsilon}_p, \hat{\boldsymbol{\epsilon}}_p)s\psi_a - \hat{h}_x^*(\boldsymbol{\eta}_p, \hat{\boldsymbol{\epsilon}}_p)\psi_a(\boldsymbol{\eta}, \boldsymbol{\epsilon}_p, \hat{\boldsymbol{\epsilon}}_p)s\psi_a \\ & + \hat{h}_y^*(\boldsymbol{\eta}_p, \hat{\boldsymbol{\epsilon}}_p)\psi_a(\boldsymbol{\eta}, \boldsymbol{\epsilon}_p, \hat{\boldsymbol{\epsilon}}_p)c\psi_a), \end{aligned} \quad (53)$$

$$\beta_3(\boldsymbol{\eta}_p, \hat{\boldsymbol{\epsilon}}_p) = \left[\hat{h}_z^*(\boldsymbol{\eta}_p, \hat{\boldsymbol{\epsilon}}_p) \right]^2 + \left[\hat{h}_x^*(\boldsymbol{\eta}_p, \hat{\boldsymbol{\epsilon}}_p)c\psi_a + \hat{h}_y^*(\boldsymbol{\eta}_p, \hat{\boldsymbol{\epsilon}}_p)s\psi_a \right]^2. \quad (54)$$

The time derivative of a longitudinal part of modified convergence vector field (44), required to calculate (51) and (52), takes the form

$$\dot{\hat{\boldsymbol{h}}}_p^*(\boldsymbol{\eta}, \boldsymbol{\epsilon}_p, \dot{\hat{\boldsymbol{\epsilon}}}_p) = \dot{\boldsymbol{h}}_p(\boldsymbol{\eta}_p, \boldsymbol{\epsilon}_p) + \delta_p \dot{\hat{\boldsymbol{\epsilon}}}_p, \quad (55)$$

while

$$\dot{\boldsymbol{h}}_p(\boldsymbol{\eta}_p, \boldsymbol{\epsilon}_p) \stackrel{(45)}{=} u_d \dot{\boldsymbol{\vartheta}}_\perp + [\dot{s}_1 \boldsymbol{\vartheta}_1 + s_1 \dot{\boldsymbol{\vartheta}}_1 + \dot{s}_2 \boldsymbol{\vartheta}_2 + s_2 \dot{\boldsymbol{\vartheta}}_2]. \quad (56)$$

The derivatives $\dot{\boldsymbol{\vartheta}}_\perp$, $\dot{\boldsymbol{\vartheta}}_j$, \dot{s}_j for $j \in \{1, 2\}$, that are present in (56), are described in detail in Appendix A. Again, to assure the output-feedback characteristics of the control structure, we propose to use the estimate of the longitudinal velocity tracking error $\hat{\boldsymbol{\epsilon}}_p$ instead of the vector $\boldsymbol{\epsilon}_p$ in the formula (50). Using this substitution, we obtain the modified version of the angular part of the convergence vector field in a form

$$\hat{\boldsymbol{h}}_o(\boldsymbol{\eta}, \hat{\boldsymbol{\epsilon}}_p, \dot{\hat{\boldsymbol{\epsilon}}}_p) = \hat{\bar{\boldsymbol{\eta}}}_{oa}(\boldsymbol{\eta}, \hat{\boldsymbol{\epsilon}}_p, \dot{\hat{\boldsymbol{\epsilon}}}_p) + \boldsymbol{K}_a \bar{\boldsymbol{e}}_a(\boldsymbol{\eta}_p, \hat{\boldsymbol{\epsilon}}_p), \quad (57)$$

where the components of $\hat{\bar{\boldsymbol{\eta}}}_{oa}(\cdot) \triangleq [\hat{\theta}_a(\cdot) \hat{\psi}_a(\cdot)]^\top$, calculated according to the formulas (52) and (51) are utilizing the estimate of the derivative of estimated longitudinal part of convergence vector field

$$\hat{\boldsymbol{h}}_p^*(\boldsymbol{\eta}_p, \hat{\boldsymbol{\epsilon}}_p, \dot{\hat{\boldsymbol{\epsilon}}}_p) = \hat{\boldsymbol{h}}_p(\boldsymbol{\eta}_p, \hat{\boldsymbol{\epsilon}}_p) + \delta_p \dot{\hat{\boldsymbol{\epsilon}}}_p, \quad (58)$$

instead of the elements of vector $\hat{\boldsymbol{h}}_p^*$ and

$$\hat{\boldsymbol{h}}_p(\boldsymbol{\eta}_p, \boldsymbol{\epsilon}_p) = u_d \hat{\boldsymbol{\vartheta}}_\perp + [\hat{s}_1 \boldsymbol{\vartheta}_1 + s_1 \hat{\boldsymbol{\vartheta}}_1 + \hat{s}_2 \boldsymbol{\vartheta}_2 + s_2 \hat{\boldsymbol{\vartheta}}_2]. \quad (59)$$

The estimates $\hat{\boldsymbol{\vartheta}}_\perp$, $\hat{\boldsymbol{\vartheta}}_j$, \hat{s}_j for $j \in \{1, 2\}$ are precisely described in Appendix A, while $\hat{\boldsymbol{\epsilon}}_p$ consists of the second elements of vectors $\hat{\boldsymbol{x}}_i$ for $i \in \{1, \dots, 6\}$ calculated in the ESO equations (32). The final form of the modified convergence vector field is described as

$$\hat{\boldsymbol{h}}_o^*(\boldsymbol{\eta}, \hat{\boldsymbol{\epsilon}}_o, \dot{\hat{\boldsymbol{\epsilon}}}_p) = \hat{\boldsymbol{h}}_o(\boldsymbol{\eta}, \hat{\boldsymbol{\epsilon}}_p, \dot{\hat{\boldsymbol{\epsilon}}}_p) + \delta_o \hat{\boldsymbol{\epsilon}}_o, \quad (60)$$

where $\hat{\boldsymbol{\epsilon}}_o = [\hat{\epsilon}_5 \hat{\epsilon}_6]^\top$, while $\delta_o \in [0, 1]$ is a design parameter, introduced to deal with a possible overcompensation of the angular velocity tracking errors.

The reduced commanded local pseudovelocity vector (42) is recalculated with the longitudinal and angular parts of the modified convergence vector field described respectively in (44) and (60), resulting in the final form

$$\begin{aligned} \bar{\boldsymbol{v}}_c &= \begin{bmatrix} u_c & q_c & r_c \end{bmatrix}^\top \\ &= \begin{bmatrix} \hat{h}_x^* c \theta c \psi + \hat{h}_y^* c \theta s \psi - \hat{h}_z^* s \theta \\ \hat{h}_\theta^* \\ \hat{h}_\psi^* c \theta \end{bmatrix} \end{aligned} \quad (61)$$

that only requires the information about the configuration $\boldsymbol{\eta}(t)$ (see Assumption 1).

A block diagram of the proposed control structure is presented in Fig. 2.

Remark 8. The elements of auxiliary orientation $\bar{\eta}_{oa}$ defined in (49), together with their derivatives presented in (52) and (51) are well determined if only $\hat{h}_x^{*2} + \hat{h}_y^{*2} \neq 0$. When the aforementioned relation is satisfied, not only a proper definition of the auxiliary orientation and its derivative is guaranteed, but also the domain $\theta_a \in (-\frac{\pi}{2}, \frac{\pi}{2})$ is preserved, in accordance with the pitch angle constraint described in the Remark 1. A non-zero value of the velocity profile u_d introduced in (11) guarantees a persistent excitation of the VFO controller, causing that the situation when $\hat{h}_x^{*2} + \hat{h}_y^{*2} = 0$ may potentially appear only in the transient stage (however, it is very rare and non-attracting). To prevent the indeterminacy of auxiliary angles, we propose to freeze the values of $\bar{\eta}_{oa}$ and $\dot{\bar{\eta}}_{oa}$ in a previous state as long as $\hat{h}_x^{*2} + \hat{h}_y^{*2} < \varepsilon$, for sufficiently small, non-zero value of ε .

4. The main result and stability analysis

4.1. Error domain dynamics of particular subsystems

To show the boundedness of the path-following errors introduced in (19), particular subsystems of the proposed control structure have to be analyzed in an appropriate order. This subsection is focused on the definition of these subsystems, and the derivation of their dynamic equations.

Let us address first the observation errors associated with the extended state observer. According to dynamics (30), and ESO equations (32), we define a combined observation error

$$\tilde{\chi} \triangleq \begin{bmatrix} \tilde{y} \\ \tilde{\epsilon} \\ \tilde{d} \end{bmatrix} \triangleq \chi - \hat{\chi} = \begin{bmatrix} y - \hat{y} \\ \epsilon - \hat{\epsilon} \\ d - \hat{d} \end{bmatrix} \in \mathbb{R}^{18}, \quad (62)$$

where $y = [y_1 \dots y_6]^\top \stackrel{(29)}{=} [x_{11} \dots x_{16}]^\top$ is the combined observer output (see (30)). The dynamics of $\tilde{\chi}$ can be written down as

$$\dot{\tilde{\chi}}(t) = - \underbrace{\begin{bmatrix} L_1 & -I & 0 \\ L_2 & 0 & -I \\ L_3 & 0 & 0 \end{bmatrix}}_{H_\chi} \tilde{\chi}(t) + \begin{bmatrix} 0 \\ 0 \\ I \end{bmatrix} \dot{d}(t), \quad (63)$$

where $L_i \triangleq \text{diag}\{l_{i1} \dots l_{i6}\}$, $i \in \{1, 2, 3\}$ are the observer gain matrices resulting from (33), while 0 and I are, respectively, the zero and identity matrices of the appropriate dimensions.

To address dynamics of the velocity error, we introduce a modified disturbance vector

$$\begin{aligned} d^* &= [d_1^* \ d_2^* \ d_3^* \ d_4^* \ d_5^* \ d_6^*]^\top \\ &\triangleq d + M_\eta^{-1} \Delta_\eta \dot{\eta}_c - M_\eta^{-1} \Delta_\eta \dot{\eta} = d + M_\eta \Delta_\eta \epsilon, \end{aligned} \quad (64)$$

where the component $M_\eta^{-1} \Delta_\eta \dot{\eta}$ corresponds to the linear part of the environmental damping (see [8]) included in the vector μ_η in (6), while $-M_\eta^{-1} \Delta_\eta \dot{\eta}_c$ allows us to describe d^* as a function of d and ϵ . Matrix $\Delta_\eta = J \Delta J^{-1}$, where

$$\Delta \triangleq \text{diag}\{\rho_u, \rho_v, \rho_w, \rho_p, \rho_q, \rho_r\}, \quad \rho_i > 0, \quad (65)$$

includes the positive damping coefficients in the body-related coordinate system $\{B\}$. It is worth noting that only the linear part of the environmental damping model was excluded from d , while the higher-order terms still reside in vector d^* .

Remark 9. Upon Assumptions 3 and 6, Remark 8, and the equations (27), (23), and (61), we may claim that the disturbance d , defined in (26), its derivative \dot{d} , and the modified total disturbance d^* from (64) are bounded in the compact set of the vehicle's state $(\eta, \dot{\eta})$ meaning that $\sup_{t \geq 0} \|d(t)\| \leq r_d$, $\sup_{t \geq 0} \|\dot{d}(t)\| \leq r_{\dot{d}}$, and $\sup_{t \geq 0} \|d^*(t)\| \leq r_{d^*}$ are satisfied for some finite $r_d, r_{\dot{d}}, r_{d^*} > 0$.

After transformations presented in Appendix B, the velocity error dynamics, described firstly in (26), can be expressed as

$$\begin{aligned} \dot{\epsilon} &= -J \underbrace{(\Gamma K + (I - \Gamma) M^{-1} \Delta)}_{H_\epsilon} J^{-1} \epsilon \\ &+ J \Gamma K J^{-1} \tilde{\epsilon} + J \Gamma J^{-1} \tilde{d} + J(I - \Gamma) J^{-1} d^* \end{aligned} \quad (66)$$

where $K \triangleq J^{-1} K_\eta J = \text{diag}\{k_1, \dots, k_6\}$ is the ADR controller gain matrix expressed in the local frame, calculated upon the matrix K_η utilized in (28).

Remark 10. Matrix H_ϵ introduced in (66) is a convex combination of the matrices K and $M^{-1} \Delta$ that are both positive definite, thus according to [16], matrix H_ϵ is positive definite itself.

Now, let us turn to the angular part of the kinematic subsystem. The equation of roll error dynamics, calculated upon (3), (38), (25) and (35), has the form

$$\dot{e}_\phi(t) = -f_\phi(e_\phi(t), \cdot) + \epsilon_1(t). \quad (67)$$

Under Assumption 8, the dynamics of an auxiliary error vector (48) can be derived using the equations (3), (38) in the form

$$\begin{aligned} \dot{\tilde{e}}_a &= \begin{bmatrix} \dot{\theta}_a - q_c + \epsilon_5 \\ \dot{\psi}_a - \frac{1}{c\beta} r_c + \epsilon_6 \end{bmatrix} \\ &\stackrel{(60),(61)}{=} \begin{bmatrix} -k_\theta e_{\theta_a} + \delta_o \tilde{\epsilon}_\theta + (1 - \delta_o) \epsilon_\theta + \tilde{\theta}_a \\ -k_\psi e_{\psi_a} + \delta_o \tilde{\epsilon}_\psi + (1 - \delta_o) \epsilon_\psi + \tilde{\psi}_a \end{bmatrix} \\ &= -K_a \bar{e}_a + \delta_o \tilde{\epsilon}_o + (1 - \delta_o) \tilde{\epsilon}_o + \tilde{\eta}_{oa} \end{aligned} \quad (68)$$

where $\bar{e}_o \triangleq [\epsilon_5 \ \epsilon_6]^\top$ is the dimensionally reduced angular velocity error, $\tilde{\epsilon}_o \triangleq [\tilde{\epsilon}_5 \ \tilde{\epsilon}_6]^\top$ is the observation inaccuracy of the reduced vector of the angular velocity error, while

$$\tilde{\eta}_{oa} = \begin{bmatrix} \tilde{\theta}_a \\ \tilde{\psi}_a \end{bmatrix} \triangleq \begin{bmatrix} \dot{\theta}_a - \hat{\theta}_a \\ \dot{\psi}_a - \hat{\psi}_a \end{bmatrix} \quad (69)$$

correspond to the difference between the nominal derivatives of auxiliary angles from (51)-(52) and the applied derivatives of auxiliary angles utilized in (57). More detailed representation of the particular elements of $\tilde{\eta}_{oa}$ is provided in Appendix C.

The dynamics of positional error e_p will be written down separately for its particular components. Knowing that the gradient of the particular level-surfaces ∇s_j and the vector $\boldsymbol{\vartheta}_\perp$, tangential

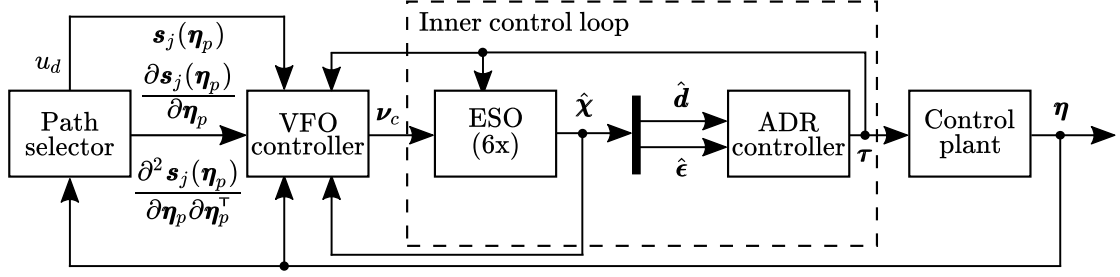


Figure 2: Block diagram of the VFO-ADR control system for the underactuated vehicle.

to the cross-section of level surfaces (see (13)) are perpendicular to each other, relation

$$\begin{aligned} & \nabla^\top s_j u_d \frac{\sigma(\nabla s_1 \times \nabla s_2)}{\|\nabla s_1 \times \nabla s_2\|} \\ & \stackrel{(44),(12)}{=} \nabla^\top s_j \hat{\mathbf{h}}_p^* + \nabla^\top s_j k_p s_1 \frac{\nabla s_1}{\|\nabla s_1\|} + \nabla^\top s_j k_p s_2 \frac{\nabla s_2}{\|\nabla s_2\|} \\ & - \nabla^\top s_j \delta_p \hat{\boldsymbol{\epsilon}}_p = 0 \end{aligned} \quad (70)$$

is always satisfied. As a consequence, we can express the level-surface dynamics as

$$\begin{aligned} \dot{s}_1 &= \nabla^\top s_1 \dot{\boldsymbol{\eta}}_p \\ &= \nabla^\top s_1 (\dot{\boldsymbol{\eta}}_{pc} - \boldsymbol{\epsilon}_p) - \nabla^\top s_1 \hat{\mathbf{h}}_p^* - k_p s_1 \|\nabla s_1\| \\ & \quad - k_p s_2 \kappa \|\nabla s_1\| + \nabla^\top s_1 \delta_p \hat{\boldsymbol{\epsilon}}_p, \end{aligned} \quad (71)$$

$$\begin{aligned} \dot{s}_2 &= \nabla^\top s_2 (\dot{\boldsymbol{\eta}}_{pc} - \boldsymbol{\epsilon}_p) - \nabla^\top s_2 \hat{\mathbf{h}}_p^* - k_p s_2 \|\nabla s_2\| \\ & \quad - k_p s_1 \kappa \|\nabla s_2\| + \nabla^\top s_2 \delta_p \hat{\boldsymbol{\epsilon}}_p, \end{aligned} \quad (72)$$

where $\kappa \angle(\nabla s_1, \nabla s_2) \neq k\pi$, $k \in \mathbb{Z}$ corresponds to the angle between gradients of level-surfaces and its value is constrained according to the Assumption 7.

4.2. Statement of the main result

Theorem 1. *Under Assumptions 1 - 8, the output-feedback VFO-ADR cascaded control law resulting from the combination of the inner-loop ADR controller (28) and the outer-loop controller, consisting of the VFO part (61) and the auxiliary roll stabilizer (35), applied into the uncertain and underactuated vehicle represented by (9), locally guarantees satisfaction of control objectives (21)-(22) for the reference path (10) with the upper bounds $\varepsilon_\eta(\omega_{oi}, \mathbf{K}_\eta, \mathbf{K}_a, k_p)$ and $\varepsilon_p(\omega_{oi}, \mathbf{K}_\eta, \mathbf{K}_a, k_p)$ such that $\varepsilon_p(\omega_{oi}, \mathbf{K}_\eta, \mathbf{K}_a, k_p \rightarrow \infty) = 0$.*

4.3. Proof of Theorem 1

Firstly, let us consider the stability of the observation error dynamics (63). The analysis will be carried out using the ISS procedure presented in [36, 15]. According to the Remark 9, the admissible domains of the observation error (62) and the perturbing input of system (63) can be defined as

$$\tilde{\boldsymbol{\chi}} \in \mathcal{D}_X, \quad \dot{\mathbf{d}} \in \mathcal{D}_D, \quad (73)$$

where $\mathcal{D}_X \triangleq \{\tilde{\boldsymbol{\chi}} \in \mathbb{R}^{18} : \|\tilde{\boldsymbol{\chi}}\| < r_X\}$, $\mathcal{D}_D \triangleq \{\dot{\mathbf{d}} \in \mathbb{R}^6 : \|\dot{\mathbf{d}}\| < r_D\}$, and $r_X, r_D > 0$. Let us introduce a positive definite function

$V_\chi \triangleq \frac{1}{2} \tilde{\boldsymbol{\chi}}^\top \tilde{\boldsymbol{\chi}}$, $V_\chi : \mathcal{D}_X \rightarrow \mathbb{R}_{\geq 0}$, such that $\alpha_{1\chi}(\|\tilde{\boldsymbol{\chi}}\|) \leq V_\chi(\tilde{\boldsymbol{\chi}}) \leq \alpha_{2\chi}(\|\tilde{\boldsymbol{\chi}}\|)$, for the limiting functions $\alpha_{1\chi}(\|\tilde{\boldsymbol{\chi}}\|) = \alpha_{2\chi}(\|\tilde{\boldsymbol{\chi}}\|) \triangleq \frac{1}{2} \|\tilde{\boldsymbol{\chi}}\|^2 \in \mathcal{K}$. A time derivative of V_χ can be assessed as

$$\begin{aligned} \dot{V}_\chi &= \tilde{\boldsymbol{\chi}}^\top \dot{\tilde{\boldsymbol{\chi}}} \stackrel{(63)}{=} -\tilde{\boldsymbol{\chi}}^\top \mathbf{H}_\chi \tilde{\boldsymbol{\chi}} + \tilde{\boldsymbol{\chi}}^\top \begin{bmatrix} \mathbf{0} \\ \mathbf{0} \\ \mathbf{I} \end{bmatrix} \dot{\mathbf{d}} \\ &\leq -(1 - \nu_\chi) \omega_o \|\tilde{\boldsymbol{\chi}}\|^2 + \|\tilde{\boldsymbol{\chi}}\| (\|\dot{\mathbf{d}}\| - \nu_\chi \omega_o \|\tilde{\boldsymbol{\chi}}\|), \end{aligned} \quad (74)$$

where $\nu_\chi \in (0, 1)$ is a majorization constant and $\omega_o = \min\{\omega_{oi} \mid i \in \{1, \dots, 6\}\}$ is the lowest eigenvalue of matrix \mathbf{H}_χ determined by the design rule (33). According to (74),

$$\dot{V}_\chi \leq -(1 - \nu_\chi) \omega_o \|\tilde{\boldsymbol{\chi}}\|^2, \quad \text{for } \|\tilde{\boldsymbol{\chi}}\| \geq \chi_\chi(\|\dot{\mathbf{d}}\|), \quad (75)$$

where

$$\chi_\chi(\|\dot{\mathbf{d}}\|) = \frac{\|\dot{\mathbf{d}}\|}{\nu_\chi \omega_o} \in \mathcal{K}. \quad (76)$$

Subsystem (63) describing the dynamics of observation errors is locally ISS with respect to perturbation $\dot{\mathbf{d}}$, that is

$$\forall t \geq 0 \quad \|\tilde{\boldsymbol{\chi}}(t)\| \leq \max \left\{ \beta_\chi(\|\tilde{\boldsymbol{\chi}}(0)\|, t), \gamma_\chi \left(\sup_{t \geq 0} \|\dot{\mathbf{d}}(t)\| \right) \right\}, \quad (77)$$

for some \mathcal{KL} -class function $\beta_\chi(\cdot, \cdot)$, where

$$\gamma_\chi = \alpha_{1\chi}^{-1}(\alpha_{2\chi}(\chi_\chi(\|\dot{\mathbf{d}}(t)\|))) = \chi_\chi(\|\dot{\mathbf{d}}(t)\|). \quad (78)$$

The result of local ISS is fulfilled within the domains (73) if the initial conditions meet the requirement $\|\tilde{\boldsymbol{\chi}}(0)\| < r_\chi = \alpha_{2\chi}^{-1}(\alpha_{1\chi}(r_X)) = r_X$, while the supreme value of the perturbation is upper-bounded by

$$\sup_{t \geq 0} \|\dot{\mathbf{d}}(t)\| < \chi_\chi^{-1}(\min\{r_\chi, \chi_\chi(r_D)\}) =: r_{\dot{\mathbf{d}}} \quad (79)$$

(see Remark 9). Formula (77) correspond to the asymptotic relation

$$\text{Is}_\infty \|\tilde{\boldsymbol{\chi}}(t)\| \leq \gamma_\chi(\text{Is}_\infty \|\dot{\mathbf{d}}(t)\|) \leq \frac{r_{\dot{\mathbf{d}}}}{\nu_\chi \omega_o}. \quad (80)$$

Hence, we can conclude the ultimate boundedness of the $\|\tilde{\boldsymbol{\chi}}(t)\|$.

Next, let us address the behaviour of velocity error $\boldsymbol{\epsilon}$, defined in (25), by analyzing subsystem (66). The norm of modified disturbance $\dot{\mathbf{d}}^*$ is bounded according to the Remark 9 and the

components of vector (62) are bounded according to the result (80), thus we can assume the existence of the compact domains

$$\boldsymbol{\epsilon} \in \mathcal{D}_E, \boldsymbol{\delta}_\epsilon \triangleq \left[\tilde{\mathbf{d}}^\top \tilde{\boldsymbol{\epsilon}}^\top \right]^\top \in \mathcal{D}_{\delta E}, \mathbf{d}^* \in \mathcal{D}_D^*, \quad (81)$$

where $\mathcal{D}_E \triangleq \{\boldsymbol{\epsilon} \in \mathbb{R}^6 : \|\boldsymbol{\epsilon}\| < r_E\}$, $\mathcal{D}_{\delta E} \triangleq \{\boldsymbol{\delta}_\epsilon \in \mathbb{R}^{12} : \|\boldsymbol{\delta}_\epsilon\| < r_{\delta E}\}$, $\mathcal{D}_D^* \triangleq \{\mathbf{d}^* \in \mathbb{R}^6 : \|\mathbf{d}^*\| < r_{D^*}\}$, and $r_E, r_{\delta E}, r_{D^*} > 0$. Let us propose the positive definite function in the form $V_\epsilon \triangleq \frac{1}{2} \boldsymbol{\epsilon}^\top \boldsymbol{\epsilon}$, $V_\epsilon : \mathcal{D}_E \rightarrow \mathbb{R}_{\geq 0}$, such that $\alpha_{1\epsilon}(\|\boldsymbol{\epsilon}\|) \leq V_\epsilon(\boldsymbol{\epsilon}) \leq \alpha_{2\epsilon}(\|\boldsymbol{\epsilon}\|)$, for the limiting functions $\alpha_{1\epsilon}(\|\boldsymbol{\epsilon}\|) = \alpha_{2\epsilon}(\|\boldsymbol{\epsilon}\|) \triangleq \frac{1}{2} \|\boldsymbol{\epsilon}\|^2 \in \mathcal{K}$. According to the velocity error dynamics (66), the time derivative of V_ϵ can be assessed as

$$\begin{aligned} \dot{V}_\epsilon &= \boldsymbol{\epsilon}^\top \dot{\boldsymbol{\epsilon}} \\ &= -\boldsymbol{\epsilon}^\top \mathbf{J} \mathbf{H}_\epsilon \mathbf{J}^{-1} \boldsymbol{\epsilon} + \boldsymbol{\epsilon}^\top \mathbf{J} \boldsymbol{\Gamma} \mathbf{K} \mathbf{J}^{-1} \tilde{\boldsymbol{\epsilon}} \\ &\quad + \boldsymbol{\epsilon}^\top \mathbf{J} \boldsymbol{\Gamma} \mathbf{J}^{-1} \tilde{\mathbf{d}} + \boldsymbol{\epsilon}^\top \mathbf{J} (\mathbf{I} - \boldsymbol{\Gamma}) \mathbf{J}^{-1} \mathbf{d}^* \\ &\leq -\lambda_{\min}(\mathbf{H}_\epsilon) \|\boldsymbol{\epsilon}\|^2 + \lambda_{\max}(\mathbf{K}) \|\boldsymbol{\epsilon}\| \|\tilde{\boldsymbol{\epsilon}}\| \\ &\quad + \|\boldsymbol{\epsilon}\| \|\tilde{\mathbf{d}}\| + \lambda_{\max}(\mathbf{I} - \boldsymbol{\Gamma}) \|\boldsymbol{\epsilon}\| \|\mathbf{d}^*\| \\ &\leq -(1 - \nu_\epsilon) \lambda_{\min}(\mathbf{H}_\epsilon) \|\boldsymbol{\epsilon}\|^2 \\ &\quad + \|\boldsymbol{\epsilon}\| \left[(1 + \lambda_{\max}(\mathbf{K})) \|\boldsymbol{\delta}_\epsilon\| + \lambda_{\max}(\mathbf{I} - \boldsymbol{\Gamma}) \|\mathbf{d}^*\| \right. \\ &\quad \left. - \nu_\epsilon \lambda_{\min}(\mathbf{H}_\epsilon) \|\boldsymbol{\epsilon}\| \right], \end{aligned} \quad (82)$$

where $\nu_\epsilon \in (0, 1)$ is a majorization constant.

Remark 11. In the calculation presented in (82), the equivalence principle of the similarity transformation have been used, i.e., the eigenvalues of \mathbf{X} are exactly the same as the eigenvalues of $\mathbf{J} \mathbf{X} \mathbf{J}^{-1}$ (see [10]), as long as the matrix \mathbf{J} has the full rank (see Remark 1).

According to (82), one can write

$$\dot{V}_\epsilon \leq -(1 - \nu_\epsilon) \lambda_{\min}(\mathbf{H}_\epsilon) \|\boldsymbol{\epsilon}\|^2 \text{ for} \quad (83)$$

$$\|\boldsymbol{\epsilon}\| \geq \chi_{1\epsilon}(\|\boldsymbol{\delta}_\epsilon\|) + \chi_{2\epsilon}(\|\mathbf{d}^*\|), \quad (84)$$

where

$$\chi_{1\epsilon}(\|\boldsymbol{\delta}_\epsilon\|) = \frac{1 + \lambda_{\max}(\mathbf{K})}{\nu_\epsilon \lambda_{\min}(\mathbf{H}_\epsilon)} \|\boldsymbol{\delta}_\epsilon\| \in \mathcal{K}, \quad (85)$$

$$\chi_{2\epsilon}(\|\mathbf{d}^*\|) = \frac{\lambda_{\max}(\mathbf{I} - \boldsymbol{\Gamma})}{\nu_\epsilon \lambda_{\min}(\mathbf{H}_\epsilon)} \|\mathbf{d}^*\| \in \mathcal{K}. \quad (86)$$

As a consequence, the velocity error subsystem is locally ISS with respect to perturbations $\boldsymbol{\delta}_\epsilon$ and \mathbf{d}^* , and

$$\begin{aligned} \forall t \geq 0 \|\boldsymbol{\epsilon}(t)\| &\leq \max \left\{ \beta_\epsilon(\|\boldsymbol{\epsilon}(0)\|, t), \gamma_{1\epsilon} \left(\sup_{t \geq 0} \|\boldsymbol{\delta}_\epsilon(t)\| \right) \right. \\ &\quad \left. + \gamma_{2\epsilon} \left(\sup_{t \geq 0} \|\mathbf{d}^*(t)\| \right) \right\}, \end{aligned} \quad (87)$$

for some \mathcal{KL} -class function $\beta_\epsilon(\cdot, \cdot)$, and functions

$$\gamma_{1\epsilon}(\|\boldsymbol{\delta}_\epsilon\|) = \alpha_{1\epsilon}^{-1}(\alpha_{2\epsilon}(\chi_{1\epsilon}(\|\boldsymbol{\delta}_\epsilon\|))) = \chi_{1\epsilon}(\|\boldsymbol{\delta}_\epsilon\|) \quad (88)$$

$$\gamma_{2\epsilon}(\|\mathbf{d}^*\|) = \alpha_{1\epsilon}^{-1}(\alpha_{2\epsilon}(\chi_{2\epsilon}(\|\mathbf{d}^*\|))) = \chi_{2\epsilon}(\|\mathbf{d}^*\|). \quad (89)$$

The result of local ISS is valid within the domains (81) if the initial condition meets the requirement $\|\boldsymbol{\epsilon}(0)\| < r_\epsilon =$

$\alpha_{2\epsilon}^{-1}(\alpha_{1\epsilon}(r_E)) = r_E$, and the supreme values of perturbations are upper-bounded by

$$\sup_{t \geq 0} \|\boldsymbol{\delta}_\epsilon(t)\| < \chi_{1\epsilon}^{-1}(\min\{r_\epsilon, \chi_{1\epsilon}(r_{\delta E})\}) =: r_{\delta\epsilon} \quad (90)$$

$$\sup_{t \geq 0} \|\mathbf{d}^*(t)\| < \chi_{2\epsilon}^{-1}(\min\{r_\epsilon, \chi_{2\epsilon}(r_{D^*})\}) =: r_{d^*}. \quad (91)$$

Formula (87) implies the asymptotic gain property

$$\begin{aligned} \text{Is}_\infty \|\boldsymbol{\epsilon}(t)\| &< \gamma_{1\epsilon}(\text{Is}_\infty \|\boldsymbol{\delta}_\epsilon(t)\|) + \gamma_{2\epsilon}(\text{Is}_\infty \|\mathbf{d}^*(t)\|) \\ &\leq \gamma_{1\epsilon}(\gamma_\chi(\text{Is}_\infty \|\tilde{\mathbf{d}}(t)\|)) + \gamma_{2\epsilon}(\text{Is}_\infty \|\mathbf{d}^*(t)\|) \\ &\leq \frac{1 + \lambda_{\max}(\mathbf{K})}{\nu_\epsilon \lambda_{\min}(\mathbf{H}_\epsilon)} \frac{1}{\nu_\chi \omega_o} r_d + \frac{\lambda_{\max}(\mathbf{I} - \boldsymbol{\Gamma})}{\nu_\epsilon \lambda_{\min}(\mathbf{H}_\epsilon)} r_{d^*}, \end{aligned} \quad (92)$$

which reveals the ultimate boundedness of the velocity error $\boldsymbol{\epsilon}(t)$. It is worth noting that for the fully-actuated vehicle $\boldsymbol{\Gamma} = \mathbf{I}$ implying $\lambda_{\max}(\mathbf{I} - \boldsymbol{\Gamma}) = 0$. In this case, the upper bound in (92) reduces to the first component.

We will now turn to the analysis of the kinematic-level subsystems. According to the equation describing the roll error dynamics (67), function $f_\phi(e_\phi, \cdot)$ should be designed with any robust control method assuring the finite-time convergence of $e_\phi(t) \rightarrow 0$, despite the perturbation $\epsilon_1(t)$. Since the result (92) shows that the signal $\epsilon_1(t)$ is bounded, a specific form of the controller (35) may be based, for example, on the sliding-mode control method (see e.g. [35]). The dynamics (68), describing the behavior of an auxiliary angular error \bar{e}_a , will be considered within some admissible domains for an auxiliary orientation error itself, and its perturbing inputs, i.e.,

$$\bar{e}_a \in \mathcal{D}_{eA}, \tilde{\boldsymbol{\epsilon}}_o \in \mathcal{D}_{\delta eA}, \bar{\boldsymbol{\epsilon}}_o \in \mathcal{D}_{\epsilon A}, \tilde{\boldsymbol{\eta}}_{oa} \in \mathcal{D}_{\eta A}, \quad (93)$$

where $\mathcal{D}_{eA} \triangleq \{\bar{e}_a \in [-\pi, \pi) \times \mathbb{R} : \|\bar{e}_a\| < r_{eA}\}$, $\mathcal{D}_{\delta eA} \triangleq \{\tilde{\boldsymbol{\epsilon}}_o \in \mathbb{R}^2 : \|\tilde{\boldsymbol{\epsilon}}_o\| < r_{\tilde{E}}\}$, $\mathcal{D}_{\epsilon A} \triangleq \{\bar{\boldsymbol{\epsilon}}_o \in \mathbb{R}^2 : \|\bar{\boldsymbol{\epsilon}}_o\| < r_E\}$, $\mathcal{D}_{\eta A} \triangleq \{\tilde{\boldsymbol{\eta}}_{oa} \in \mathbb{R}^2 : \|\tilde{\boldsymbol{\eta}}_{oa}\| < r_{\eta A}\}$, and $r_{eA}, r_{\delta eA}, r_E, r_{\eta A} > 0$. A positive definite function $V_a : \mathcal{D}_{eA} \rightarrow \mathbb{R}_{\geq 0}$ is proposed in a form $V_a \triangleq \frac{1}{2} \bar{\mathbf{e}}_a^\top \bar{\mathbf{e}}_a$, such that $\alpha_{1a}(\|\bar{e}_a\|) \leq V_a(\bar{e}_a) \leq \alpha_{2a}(\|\bar{e}_a\|)$ for the limiting functions $\alpha_{1a}(\|\bar{e}_a\|) = \alpha_{2a}(\|\bar{e}_a\|) \triangleq \frac{1}{2} \|\bar{e}_a\|^2 \in \mathcal{K}$. The time derivative of function V_a can be assessed as follows:

$$\begin{aligned} \dot{V}_a &= \bar{\mathbf{e}}_a^\top \dot{\bar{\mathbf{e}}}_a \\ &\stackrel{(68)}{=} -\bar{\mathbf{e}}_a^\top \mathbf{K}_a \bar{\mathbf{e}}_a + \bar{\mathbf{e}}_a^\top \delta_o \tilde{\boldsymbol{\epsilon}}_o + \bar{\mathbf{e}}_a^\top (1 - \delta_o) \bar{\boldsymbol{\epsilon}}_o + \bar{\mathbf{e}}_a^\top \tilde{\boldsymbol{\eta}}_{oa} \\ &\leq -\lambda_{\min}(\mathbf{K}_a) \|\bar{e}_a\|^2 + \|\bar{e}_a\| \left[\delta_o \|\tilde{\boldsymbol{\epsilon}}_o\| \right. \\ &\quad \left. + (1 - \delta_o) \|\bar{\boldsymbol{\epsilon}}_o\| + \|\tilde{\boldsymbol{\eta}}_{oa}\| \right] \\ &= -(1 - \nu_a) \lambda_{\min}(\mathbf{K}_a) \|\bar{e}_a\|^2 + \|\bar{e}_a\| \left[\delta_o \|\tilde{\boldsymbol{\epsilon}}_o\| \right. \\ &\quad \left. + (1 - \delta_o) \|\bar{\boldsymbol{\epsilon}}_o\| + \|\tilde{\boldsymbol{\eta}}_{oa}\| - \nu_a \lambda_{\min}(\mathbf{K}_a) \|\bar{e}_a\| \right], \end{aligned} \quad (94)$$

where $\nu_a \in (0, 1)$ is a majorization factor. According to (94), one concludes

$$\dot{V}_a \leq -(1 - \nu_a) \lambda_{\min}(\mathbf{K}_a) \|\bar{e}_a\|^2 \text{ for} \quad (95)$$

$$\|\bar{e}_a\| \geq \chi_{1a}(\|\tilde{\boldsymbol{\epsilon}}_o\|) + \chi_{2a}(\|\bar{\boldsymbol{\epsilon}}_o\|) + \chi_{3a}(\|\tilde{\boldsymbol{\eta}}_{oa}\|), \quad (96)$$

where

$$\chi_{1a}(\|\tilde{\bar{\epsilon}}_o\|) = \frac{\delta_o}{\nu_a \lambda_{\min}(\mathbf{K}_a)} \|\tilde{\bar{\epsilon}}_o\| \in \mathcal{K}, \quad (97)$$

$$\chi_{2a}(\|\tilde{\bar{\epsilon}}_o\|) = \frac{(1 - \delta_o)}{\nu_a \lambda_{\min}(\mathbf{K}_a)} \|\tilde{\bar{\epsilon}}_o\| \in \mathcal{K}, \quad (98)$$

$$\chi_{3a}(\|\tilde{\bar{\eta}}_{oa}\|) = \frac{1}{\nu_a \lambda_{\min}(\mathbf{K}_a)} \|\tilde{\bar{\eta}}_{oa}\| \in \mathcal{K}. \quad (99)$$

Thus, subsystem describing dynamics of error \bar{e}_a is locally ISS with respect to the inputs $\tilde{\bar{\epsilon}}_o$, $\bar{\epsilon}_o$ and $\tilde{\bar{\eta}}_{oa}$. It implies

$$\begin{aligned} \forall t \geq 0 \|\bar{e}_a(t)\| \leq & \max \left\{ \beta_a(\|\bar{e}_a(0)\|, t), \gamma_{1a} \left(\sup_{t \geq 0} \|\tilde{\bar{\epsilon}}_o(t)\| \right) \right. \\ & \left. + \gamma_{2a} \left(\sup_{t \geq 0} \|\bar{\epsilon}_o(t)\| \right) + \gamma_{3a} \left(\sup_{t \geq 0} \|\tilde{\bar{\eta}}_{oa}(t)\| \right) \right\} \end{aligned} \quad (100)$$

for some function $\beta_a(\cdot, \cdot)$ of class \mathcal{KL} , and for

$$\gamma_{1a}(\|\tilde{\bar{\epsilon}}_o\|) = \alpha_{1a}^{-1}(\alpha_{2a}(\chi_{1a}(\|\tilde{\bar{\epsilon}}_o(t)\|))) = \chi_{1a}(\|\tilde{\bar{\epsilon}}_o(t)\|), \quad (101)$$

$$\gamma_{2a}(\|\bar{\epsilon}_o\|) = \alpha_{1a}^{-1}(\alpha_{2a}(\chi_{2a}(\|\bar{\epsilon}_o(t)\|))) = \chi_{2a}(\|\bar{\epsilon}_o(t)\|), \quad (102)$$

$$\gamma_{3a}(\|\tilde{\bar{\eta}}_{oa}\|) = \alpha_{1a}^{-1}(\alpha_{2a}(\chi_{3a}(\|\tilde{\bar{\eta}}_{oa}(t)\|))) = \chi_{3a}(\|\tilde{\bar{\eta}}_{oa}(t)\|). \quad (103)$$

The local ISS result is valid within the domains defined in (93) if the initial auxiliary orientation error satisfies the inequality

$$\|\bar{e}_a(0)\| < r_{ea} = \alpha_{2a}^{-1}(\alpha_{1a}(r_{ea})) = r_{ea} \quad (104)$$

and the norms of disturbing vectors are upper bounded by

$$\sup_{t \geq 0} \|\tilde{\bar{\epsilon}}_o(t)\| < r_{\tilde{\bar{\epsilon}}} = \chi_{1a}^{-1}(\min\{r_{ea}, \chi_{1a}(r_{\tilde{\bar{\epsilon}}})\}) \quad (105)$$

$$\sup_{t \geq 0} \|\bar{\epsilon}_o(t)\| < r_e = \chi_{2a}^{-1}(\min\{r_{ea}, \chi_{2a}(r_e)\}) \quad (106)$$

$$\sup_{t \geq 0} \|\tilde{\bar{\eta}}_{oa}(t)\| < r_{\eta a} = \chi_{3a}^{-1}(\min\{r_{ea}, \chi_{3a}(r_{\eta a})\}). \quad (107)$$

Inequality (100) implies the asymptotic relation

$$\begin{aligned} \text{ls}_{\infty} \|\bar{e}_a(t)\| & < \gamma_{1a}(\text{ls}_{\infty} \|\tilde{\bar{\epsilon}}_o(t)\|) \\ & + \gamma_{2a}(\text{ls}_{\infty} \|\bar{\epsilon}_o(t)\|) + \gamma_{3a}(\text{ls}_{\infty} \|\tilde{\bar{\eta}}_{oa}(t)\|) \\ & \leq \gamma_{1a}(\text{ls}_{\infty} \|\tilde{\bar{\chi}}(t)\|) + \gamma_{2a}(\text{ls}_{\infty} \|\epsilon(t)\|) \\ & + \gamma_{3a}(\sup_{t \geq 0} (|f_{\psi}(t)| |f_h(t)| + |f_{\theta}(t)| |f_h(t)|) \text{ls}_{\infty} \|\tilde{\bar{\chi}}(t)\|) \\ & \leq \frac{\delta_o}{\nu_a \lambda_{\min}(\mathbf{K}_a)} \frac{1}{\nu_{\chi} \omega_o} r_d \\ & + \frac{1 - \delta_o}{\nu_a \lambda_{\min}(\mathbf{K}_a)} \left[\frac{1 + \lambda_{\max}(\mathbf{K})}{\nu_{\epsilon} \lambda_{\min}(\mathbf{H}_{\epsilon})} \frac{1}{\nu_{\chi} \omega_o} r_d \right. \\ & \left. + \frac{\lambda_{\max}(\mathbf{I} - \mathbf{\Gamma})}{\nu_{\epsilon} \lambda_{\min}(\mathbf{H}_{\epsilon})} r_{d^*} \right] \\ & + \frac{1}{\nu_a \lambda_{\min}(\mathbf{K}_a)} \sup_{t \geq 0} (|f_{\psi}(t)| |f_h(t)| + |f_{\theta}(t)| |f_h(t)|) \frac{1}{\nu_{\chi} \omega_o} r_d \\ & =: r_{ea}^{\infty}. \end{aligned} \quad (108)$$

We can conclude the ultimate boundedness of an auxiliary orientation error norm $\|\bar{e}_a(t)\|$. Functions $|f_h(t)|$, $|f_{\theta}(t)|$ and $|f_{\psi}(t)|$ result from the analysis presented in Appendix C. Note that

theoretically, for $\delta_o = 1$, the second component of the ultimate upper bound (108) is equal to zero, excluding the potential influence on the quality of the control accuracy caused by the system underactuation.

Now let us analyze the boundedness of position error (19) upon the dynamics (71)-(72). The predefined domain for the position error is determined by

$$\mathbf{e}_p \in \mathcal{D}_{eP}, \quad (109)$$

where $\mathcal{D}_{eP} \triangleq \{\mathbf{e}_p \in \mathbb{R}^2 : \|\mathbf{e}_p\| < r_{eP}\}$ for $r_{eP} > 0$. Let us also define the domains related to the perturbing vectors as

$$\delta_{eP} \triangleq [\bar{\mathbf{e}}_a^{\top} \bar{\boldsymbol{\epsilon}}_p^{\top}]^{\top} \in \mathcal{D}_{\delta eP}, \quad (110)$$

$$\delta_{\epsilon P} \triangleq [\bar{\mathbf{e}}_a^{\top} \boldsymbol{\epsilon}_p^{\top}]^{\top} \in \mathcal{D}_{\delta \epsilon P}, \quad (111)$$

$$\bar{\mathbf{e}}_a \in \mathcal{D}_{eA}, \quad (112)$$

where $\mathcal{D}_{\delta eP} \triangleq \{\delta_{eP} \in [-\pi, \pi) \times \mathbb{R}^4 : \|\delta_{eP}\| < r_{\delta eP}\}$, $\mathcal{D}_{\delta \epsilon P} \triangleq \{\delta_{\epsilon P} \in [-\pi, \pi) \times \mathbb{R}^4 : \|\delta_{\epsilon P}\| < r_{\delta \epsilon P}\}$, $\mathcal{D}_{eA} \triangleq \{\bar{\mathbf{e}}_a \in [-\pi, \pi) \times \mathbb{R} : \|\bar{\mathbf{e}}_a\| < r_{eA}\}$, and $r_{\delta eP}$, $r_{\delta \epsilon P}$, $r_{eA} > 0$. Vectors assigned to the particular domains in (110)-(112) are bounded upon the results (80), (92), and (108). Let us propose the positive definite function

$$\begin{aligned} V_p & \triangleq 2 \int_0^{\mathbf{e}_p} \begin{bmatrix} s_1 \\ \frac{s_1}{\|\nabla s_1\|} \\ \frac{s_2}{\|\nabla s_2\|} \end{bmatrix}^{\top} d\mathbf{e}_p \\ & = 2 \int_0^{\mathbf{e}_p} \left(\frac{s_1}{\|\nabla s_1\|} ds_1 + \frac{s_2}{\|\nabla s_2\|} ds_2 \right). \end{aligned} \quad (113)$$

Under Assumption 5, there exists a lower-bound of the V_p function, i.e.,

$$\begin{aligned} & \int_0^{s_1} \frac{\lambda}{\|\nabla s_1(\lambda)\|} d\lambda + \int_0^{s_2} \frac{\lambda}{\|\nabla s_2(\lambda)\|} d\lambda \\ & > \int_0^{s_1} \frac{\lambda}{\bar{m}_1} d\lambda + \int_0^{s_2} \frac{\lambda}{\bar{m}_2} d\lambda = \frac{1}{2\bar{m}_1} s_1^2 + \frac{1}{2\bar{m}_2} s_2^2, \end{aligned} \quad (114)$$

implying that the function $V_p : \mathcal{D}_{eP} \rightarrow \mathbb{R}_{\geq 0}$ satisfies the requirement of being positive definite always, except $V_p = 0$ for $\mathbf{e}_p = \mathbf{0}$. By referring to Assumption 5, one may verify that to satisfy the inequality $\alpha_{1p}(\|\mathbf{e}_p\|) \leq V_p(\mathbf{e}_p) \leq \alpha_{2p}(\|\mathbf{e}_p\|)$, the limiting functions α_{1p} , α_{2p} can be defined as

$$\alpha_{1p}(\|\mathbf{e}_p\|) \triangleq \sqrt{\frac{\bar{m}_1^2 + \bar{m}_2^2}{\bar{m}_1^2 \bar{m}_2^2}} \|\mathbf{e}_p\|^2 \in \mathcal{K}, \quad (115)$$

$$\alpha_{2p}(\|\mathbf{e}_p\|) \triangleq \sqrt{\frac{m_1^2 + m_2^2}{\bar{m}_1^2 \bar{m}_2^2}} \|\mathbf{e}_p\|^2 \in \mathcal{K}. \quad (116)$$

The upper bound of \dot{V}_p has been derived in Appendix D, and takes the form

$$\begin{aligned} \dot{V}_p & = \frac{1}{\|\nabla s_1\|} s_1 \dot{s}_1 + \frac{1}{\|\nabla s_2\|} s_2 \dot{s}_2 \\ & \leq -k_p(1 - \nu_p) \mathbf{e}_p^{\top} \lambda_{\min}(\mathbf{H}_p) \mathbf{e}_p + \|\mathbf{e}_p\| \left[2(1 - \delta_p) \|\boldsymbol{\epsilon}_p\| \right. \\ & \quad \left. + 2\delta_p \|\tilde{\bar{\epsilon}}_p\| + 2\sqrt{7}|u_d| \|\bar{\mathbf{e}}_a\| + 2\sqrt{7}\delta_p(\|\boldsymbol{\epsilon}_p\| + \|\tilde{\bar{\epsilon}}_p\|) \|\bar{\mathbf{e}}_a\| \right. \\ & \quad \left. - k_p \|\mathbf{e}_p\| (\lambda_{\min}(\mathbf{H}_p) \nu_p - 2\sqrt{7} \|\bar{\mathbf{e}}_a\|) \right], \end{aligned} \quad (117)$$

where $\nu_p \in (0, 1)$ is a majorization constant, $\mathbf{H}_p = [1 \ \kappa; \kappa \ 1]$ is a positive-definite matrix (see Assumption 7), and $\lambda_{\min}(\mathbf{H}_p) = (1 - |\kappa|)$. According to the inequality (117), one can write

$$\dot{V}_p \leq -k_p \lambda_{\min}(\mathbf{H}_p) \|\mathbf{e}_p\|^2 \text{ for} \quad (118)$$

$$\|\mathbf{e}_p\| \geq \chi_{1p}(\|\delta_{ep}\|) + \chi_{2p}(\|\delta_{ep}\|) + \chi_{3p}(\|\bar{\mathbf{e}}_a\|), \quad (119)$$

where the functions

$$\chi_{1p}(\|\delta_{ep}\|) = \frac{2(1 - \delta_p)\|\delta_{ep}\| + 2\sqrt{7}\delta_p\|\delta_{ep}\|^2}{k_p(\lambda_{\min}(\mathbf{H}_p)\nu_p - 2\sqrt{7}\|\delta_{ep}\|)}, \quad (120)$$

$$\chi_{2p}(\|\delta_{ep}\|) = \frac{2\delta_p\|\delta_{ep}\| + 2\sqrt{7}\delta_p\|\delta_{ep}\|^2}{k_p(\lambda_{\min}(\mathbf{H}_p)\nu_p - 2\sqrt{7}\|\delta_{ep}\|)}, \quad (121)$$

$$\chi_{3p}(\|\bar{\mathbf{e}}_a\|) = \frac{2\sqrt{7}|u_d|\|\bar{\mathbf{e}}_a\|}{k_p(\lambda_{\min}(\mathbf{H}_p)\nu_p - 2\sqrt{7}\|\bar{\mathbf{e}}_a\|)}, \quad (122)$$

are locally functions of class \mathcal{K} for $\|\delta_{ep}\| < \nu_p \lambda_{\min}(\mathbf{H}_p)/2\sqrt{7}$, $\|\delta_{ep}\| < \nu_p \lambda_{\min}(\mathbf{H}_p)/2\sqrt{7}$, and $\|\bar{\mathbf{e}}_a\| < \nu_p \lambda_{\min}(\mathbf{H}_p)/2\sqrt{7}$. The latter constraints determine the values of constants $r_{\delta ep}$, $r_{\delta eP}$, and r_{eA} , used in definitions of the domains $\mathcal{D}_{\delta ep}$, $\mathcal{D}_{\delta eP}$ and \mathcal{D}_{eA} introduced in (110)-(112).

According to (118), the subsystem describing the position error dynamics is locally ISS with respect to the disturbing inputs δ_{ep} , δ_{eP} and $\bar{\mathbf{e}}_a$, that is,

$$\forall t \geq 0 \|\mathbf{e}_p(t)\| \leq \max\left\{\beta_p(\|\mathbf{e}_p(0)\|, t), \gamma_{1p}\left(\sup_{t \geq 0} \|\delta_{ep}(t)\|\right) + \gamma_{2p}\left(\sup_{t \geq 0} \|\delta_{eP}(t)\|\right) + \gamma_{3p}\left(\sup_{t \geq 0} \|\bar{\mathbf{e}}_a(t)\|\right)\right\} \quad (123)$$

for some $\beta_p(\cdot, \cdot)$ function of class \mathcal{KL} , and for

$$\begin{aligned} \gamma_{1p}(\|\delta_{ep}\|) &= \alpha_{1p}^{-1}(\alpha_{2p}(\chi_{1p}(\|\delta_{ep}(t)\|))) \\ &= \frac{\sqrt{2}}{2} \sqrt[4]{\frac{\bar{m}_1^2 \bar{m}_2^2}{\bar{m}_1^2 + \bar{m}_2^2}} \sqrt{\frac{m_1^2 + m_2^2}{\bar{m}_1^2 \bar{m}_2^2}} \chi_{1p}(\|\delta_{ep}(t)\|), \end{aligned} \quad (124)$$

$$\begin{aligned} \gamma_{2p}(\|\delta_{ep}\|) &= \alpha_{1p}^{-1}(\alpha_{2p}(\chi_{2p}(\|\delta_{ep}(t)\|))) \\ &= \frac{\sqrt{2}}{2} \sqrt[4]{\frac{\bar{m}_1^2 \bar{m}_2^2}{\bar{m}_1^2 + \bar{m}_2^2}} \sqrt{\frac{m_1^2 + m_2^2}{\bar{m}_1^2 \bar{m}_2^2}} \chi_{2p}(\|\delta_{ep}(t)\|), \end{aligned} \quad (125)$$

$$\begin{aligned} \gamma_{3p}(\|\bar{\mathbf{e}}_a\|) &= \alpha_{1p}^{-1}(\alpha_{2p}(\chi_{3p}(\|\bar{\mathbf{e}}_a(t)\|))) \\ &= \frac{\sqrt{2}}{2} \sqrt[4]{\frac{\bar{m}_1^2 \bar{m}_2^2}{\bar{m}_1^2 + \bar{m}_2^2}} \sqrt{\frac{m_1^2 + m_2^2}{\bar{m}_1^2 \bar{m}_2^2}} \chi_{3p}(\|\bar{\mathbf{e}}_a(t)\|). \end{aligned} \quad (126)$$

The ISS result is valid within the domains defined in (109)-(112) if the initial error satisfies

$$\begin{aligned} \|\mathbf{e}_p(0)\| &< r_{ep} = \alpha_{2p}^{-1}(\alpha_{1p}(r_{ep})) \\ &= \frac{\sqrt{2}}{2} \sqrt[4]{\frac{m_1^2 m_2^2}{\bar{m}_1^2 + \bar{m}_2^2}} \sqrt{\frac{\bar{m}_1^2 + \bar{m}_2^2}{\bar{m}_1^2 \bar{m}_2^2}} r_{ep}, \end{aligned} \quad (127)$$

and the disturbing terms are bounded by

$$\sup_{t \geq 0} \|\delta_{ep}(t)\| < r_{\delta ep} = \chi_{1p}^{-1}(\min\{r_{ep}, \chi_{1p}(r_{\delta ep})\}), \quad (128)$$

$$\sup_{t \geq 0} \|\delta_{eP}(t)\| < r_{\delta eP} = \chi_{2p}^{-1}(\min\{r_{ep}, \chi_{2p}(r_{\delta eP})\}), \quad (129)$$

$$\sup_{t \geq 0} \|\bar{\mathbf{e}}_a(t)\| < r_{ap} = \chi_{3p}^{-1}(\min\{r_{ep}, \chi_{3p}(r_{ea})\}). \quad (130)$$

The final result concerning the boundedness of position error can be expressed by referring to the asymptotic gain property, i.e.,

$$\begin{aligned} \text{Is}_{\infty} \|\mathbf{e}_p(t)\| &\leq \gamma_{1p}(\text{Is}_{\infty} \|\delta_{ep}(t)\|) \\ &+ \gamma_{2p}(\text{Is}_{\infty} \|\delta_{eP}(t)\|) + \gamma_{3p}(\text{Is}_{\infty} \|\bar{\mathbf{e}}_a(t)\|) =: \varepsilon_p. \end{aligned} \quad (131)$$

According to (124)-(126), the ultimate upper bound of the position error determined by (131) can be made arbitrarily small for the large enough value of gain k_p .

Finally, we will discuss the terminal behaviour of the angular error component introduced in (20). Under Assumption 8, we limit an analysis to the behavior of the orientation error $\mathbf{e}_o(\boldsymbol{\eta}_p) \bmod 2\pi$ reduced to the pitch- and yaw-related components.

To present the terminal boundedness of the yaw error e_{ψ} , let us introduce the difference

$$\varepsilon_{\psi} \triangleq \psi_d - \psi_a^* = \psi_d - \text{Atan2}(s\psi_a, c\psi_a), \quad (132)$$

where ψ_a^* corresponds to the angle ψ_a limited to the $[-\pi, \pi]$ range. Based on the transformations presented in Appendix E, we can conservatively assess what follows

$$|\varepsilon_{\psi}| \leq f_{\varepsilon_{\psi}} \text{ for} \quad (133)$$

$$\begin{aligned} f_{\varepsilon_{\psi}} &= \text{Atan2}(2k_p \|\mathbf{e}_p\| + \delta_p \|\boldsymbol{\epsilon}_p\| + \delta_p \|\bar{\boldsymbol{\epsilon}}_p\|, \\ &|u_d \|\bar{\boldsymbol{\vartheta}}_{\perp}\|^2 - k_p s_1 \bar{\boldsymbol{\vartheta}}_1^{\top} \bar{\boldsymbol{\vartheta}}_{\perp} - k_p s_2 \bar{\boldsymbol{\vartheta}}_2^{\top} \bar{\boldsymbol{\vartheta}}_{\perp} + \delta_p \hat{\boldsymbol{\epsilon}}_o^{\top} \bar{\boldsymbol{\vartheta}}_{\perp}|), \end{aligned} \quad (134)$$

where $\bar{\boldsymbol{\vartheta}}_{\perp} = [\vartheta_{\perp x} \ \vartheta_{\perp y}]^{\top}$.

Remark 12. According to the physical interpretation of subsystem (66) and to the definition (25), it is impossible to obtain $f_{\varepsilon_{\psi}} = 0$ for the underactuated vehicle. Even in the case when $\mathbf{e}_p = \mathbf{0}$, values of the longitudinal velocity errors associated with the non-actuated axes will have a non-zero values resulting in the vehicle's slide directly along the path. A similar observation was made for the wheeled vehicles in [38].

In view of the results (80), (92), and (131) and referring to Remark 3, the boundary condition presented in (133) is in the domain $\varepsilon_{\psi} \in (0, \frac{\pi}{2}]$, and $|\varepsilon_{\psi}|$ decreases with the decreasing values of $\|\mathbf{e}_p\|$, $\|\boldsymbol{\epsilon}_p\|$, and $\|\bar{\boldsymbol{\epsilon}}_p\|$. Finally, the ultimate bound of $|\varepsilon_{\psi}|$ can be written down as

$$\text{Is}_{\infty} |\varepsilon_{\psi}(t)| \leq \text{Is}_{\infty} f_{\varepsilon_{\psi}}(t) =: r_{\varepsilon_{\psi}}^{\infty}. \quad (135)$$

According to (20), (49) and (132), we can express the yaw angle error as $e_{\psi} = \psi_d - \psi_a^* + \psi_a - \psi + \psi_a^* - \psi_a = \varepsilon_{\psi} + e_{\psi a} + 2k\pi$, thus

$$e_{\psi}(t) \bmod 2\pi = \varepsilon_{\psi} + e_{\psi a}. \quad (136)$$

The ultimate value of e_ψ is upper bounded by

$$\begin{aligned} \text{Is}_\infty|e_\psi(t) \bmod 2\pi| &\leq \text{Is}_\infty|\varepsilon_\psi| + \text{Is}_\infty|e_{\psi a}| \\ &\leq \text{Is}_\infty|\varepsilon_\psi| + \text{Is}_\infty\|\bar{e}_a\| \\ &= r_{\varepsilon\psi}^\infty + r_{ea}^\infty, \end{aligned} \quad (137)$$

where $r_{\varepsilon\psi}^\infty$ and r_{ea}^∞ were respectively introduced in (135) and (108).

Let us now move to the analysis of the pitch angle error e_θ , beginning with the introduction of a difference

$$\begin{aligned} \varepsilon_\theta &\triangleq \theta_d - \theta_a \\ &= \arctan\left(\frac{\hat{h}_z^*\|\bar{\vartheta}_\perp\| - \vartheta_{\perp z}\sqrt{\hat{h}_x^{*2} + \hat{h}_y^{*2}}}{\|\bar{\vartheta}_\perp\|\sqrt{\hat{h}_x^{*2} + \hat{h}_y^{*2}} + \hat{h}_z^*\vartheta_{\perp z}}\right) \end{aligned} \quad (138)$$

derived in Appendix F. Recalling (44), after some algebraic calculations, one can write down that

$$|\varepsilon_\theta| \leq \arctan\left(\frac{\beta_4}{\beta_5}\right) =: f_{\varepsilon\theta} \in \left[0, \frac{\pi}{2}\right), \quad (139)$$

for

$$\begin{aligned} \beta_4 &= 4\delta_p^2\left(\|\varepsilon_p\| + \|\bar{\varepsilon}_p\|\right)^2 + 16k_p\delta_p\left(\|\varepsilon_p\| + \|\bar{\varepsilon}_p\|\right)\|e_p\| \\ &\quad + 16k_p^2\|e_p\|^2 + 8u_d\delta_p\left(\|\varepsilon_p\| + \|\bar{\varepsilon}_p\|\right) + 16u_dk_p\|e_p\| \\ \beta_5 &= \left\|\left(\|\bar{\vartheta}_\perp\|\sqrt{\hat{h}_x^{*2} + \hat{h}_y^{*2}} + \hat{h}_z^*\vartheta_{\perp z}\right)\right. \\ &\quad \left.\cdot\left(\hat{h}_z^*\|\bar{\vartheta}_\perp\| + \vartheta_{\perp z}\sqrt{\hat{h}_x^{*2} + \hat{h}_y^{*2}}\right)\right\|. \end{aligned}$$

The value of ε_θ decreases with the decrease of $\|e_p\|$, $\|\varepsilon_p\|$, and $\|\bar{\varepsilon}_p\|$ and according to (80), (92), and (131), its ultimate upper bound can be designated as

$$\text{Is}_\infty|\varepsilon_\theta(t)| \leq \text{Is}_\infty f_{\varepsilon\theta}(t) =: r_{\varepsilon\theta}^\infty. \quad (140)$$

Upon the result (140), we can state that the pitch angle error

$$e_\theta = \theta_d - \theta_a + \theta_a - \theta = \varepsilon_\theta + e_{\theta a} \quad (141)$$

is ultimately bounded by

$$\begin{aligned} \text{Is}_\infty|e_\theta(t)| &\leq \text{Is}_\infty|\varepsilon_\theta(t)| + \text{Is}_\infty|e_{\theta a}(t)| \\ &\leq \text{Is}_\infty|\varepsilon_\theta(t)| + \text{Is}_\infty\|\bar{e}_a(t)\| \\ &\leq r_{\varepsilon\theta}^\infty + r_{ea}^\infty, \end{aligned} \quad (142)$$

where $r_{\varepsilon\theta}^\infty$ and r_{ea}^∞ were introduced in (140) and (108), respectively.

Recalling the control objective from (21), according to the results (131), (137), (142), and upon Assumption 8, error $e_{2\pi}$ defined in (20) satisfies

$$\begin{aligned} \text{Is}_\infty\|e_{2\pi}(t)\| &\leq \text{Is}_\infty\|e_p(t)\|_1 + \text{Is}_\infty\|e_o(t) \bmod 2\pi\|_1 \\ &\leq \sqrt{2}\text{Is}_\infty\|e_p(t)\| + \text{Is}_\infty|e_\phi(t)| \\ &\quad + \text{Is}_\infty|e_\theta(t)| + \text{Is}_\infty|e_\psi(t) \bmod 2\pi| \\ &\leq \sqrt{2}\varepsilon_p + r_\phi^\infty + r_{\varepsilon\psi}^\infty + r_{\varepsilon\theta}^\infty + 2r_{ea}^\infty =: \varepsilon_\eta \end{aligned} \quad (143)$$

where $\|\cdot\|_1$ is the 1-norm of a vector, and the ultimate upper bound $r_\phi^\infty = 0$ in the view of the Assumption 8. Result (143) completes the proof of Theorem 1.

Table 1: Values of the design parameters selected for simulations of the VFO-ADR controller.

Parameter	Value
\mathbf{K}	diag{6 6 6 15 15 15}
$\hat{\mathbf{B}}$	diag{2.5 0.75 0.75 0.3 0.3 0.3}
ω_{oi}	80
k_ϕ	5
k_p	2
k_θ	4
k_ψ	4
ξ_d	1
δ_p	0.8
δ_o	1.0

5. Simulation results

The simulation study of the described control structure was conducted with the mathematical model of an underactuated, ellipsoidally-shaped rigid-body vehicle (modeled according to [8] and equations (6)-(7)), implemented in the Matlab/Simulink environment. Actuation structure of the vehicle was determined by selecting the input matrix $\mathbf{\Gamma} = \text{diag}\{1 \ 0 \ 0 \ 1 \ 1 \ 1\}$, implying underactuation along y^B and z^B axes. A helix-like reference path utilized in this case study was defined with the level-surface equations $s_1(\boldsymbol{\eta}_p) = -x + \sin(4z) = 0$ and $s_2(\boldsymbol{\eta}_p) = -y + \cos(4z) = 0$, the reference velocity along the path was set to $u_d = 0.1$ m/s, while the direction along the path was determined by $\sigma = 1$. The simulation time horizon $T_s = 100$ s, and the initial conditions were set to $\boldsymbol{\eta}(0) = [\pi/6 \ -\pi/3 \ \pi/4 \ 1.0 \ 2.0 \ 0.5]^\top$, $\dot{\boldsymbol{\eta}}(0) = \mathbf{0}$, and $\hat{\mathbf{x}}_i(0) = [-\eta_i(0) \ 0 \ 0]^\top$ (all in the appropriate SI units). A list of parameter values selected for the VFO-ADR controller is presented in the Table 1. The feedback function of an auxiliary roll controller introduced in (35) were chosen to be in a form $f_\phi(e_\phi, \cdot) = -k_\phi\phi(t)$. Choosing this control function assures a practical stability of the equilibrium point $e_\phi = 0$, i.e. $\text{Is}_\infty|e_\phi(t)| < \delta_\phi$. In this way, we want to present the conservativeness of the Assumption 8 which is not necessary to obtain a satisfying control performance. During the first 50 s of simulation, the vehicle was controlled with the basic VFO controller presented in [20] (obtained by setting $\delta_o = \delta_p = 0$ in (44) and (60)) and after this time, the kinematic-level controller was switched to the proposed VFO controller with values of δ_o and δ_p set to the ones from Table 1. To preserve continuity of control signals, the transition between values of parameters δ_o and δ_p was forced by modulation with a step response of the low pass filter $G(s) = 1/(9s^2 + 6s + 1)$. To avoid extremely large values of the control signals at the beginning of simulation, the controller actions were turned off during the first second of simulation (see [13]), so the initial peaking phenomenon didn't make any impact on the presented results. To keep the control signal $\boldsymbol{\tau}$ values on a reasonable level (that is, a feasible level for actuators implemented on a small mobile vehicle), we have scaled the commanded velocities $\bar{\mathbf{v}}_c$ from (61) with the procedure taken from [22].

Results of the conducted simulation are presented in Fig. 3 and in Table 2. To the spatial representation of a vehicle path

Table 2: Obtained average values of particular signals in the specific time intervals (signals expressed in the SI units).

-	$t \in (40, 50]$ s	$t \in (90, 100]$ s
$\ e_p\ _{avg}$	0.0865	0.0083
$\ e_o\ _{avg}$	0.5375	0.5750
$ e_\phi _{avg}$	0.0001	< 0.0001
$ e_{\theta a} _{avg}$	2.0562	0.0117
$ e_{\psi a} _{avg}$	1.0280	0.0063
$\ v_c\ _{avg}$	0.2043	0.1340
$\ \Gamma\tau\ _{avg}$	0.2313	0.0906

visible on the first plot in Fig. 3, we have added a small coordinate systems representing the attitude of the body-fixed frame $\{B\}$ in each second. Signals τ_v and τ_w are cut out by the selected Γ matrix, and thus are not presented in the figures. To calculate the average values of particular signals presented in Table 2, we used the formula $\alpha_{avg} = \frac{1}{t_2 - t_1} \int_{t_1}^{t_2} \alpha(t) dt$ for an exemplary signal α and time interval $t \in [t_1, t_2]$.

After the initial transient stage, the dynamical system reached a first steady motion conditions around $t = 20$ s, for the proposed VFO controller with $\delta_p = \delta_o = 0$. After $t = 50$ s, the drift compensation coefficients δ_o , δ_p were smoothly changed to the values from Table 1 and the final steady motion conditions were obtained around time instant $t = 65$ s. The drift compensation component of the VFO controller introduced in this article has significantly improved the control performance of the vehicle position subsystem, decreasing the average value of position error $\|e_p\|$ by the factor of 10. Although the auxiliary orientation errors $|e_{\theta a}|$ and $|e_{\psi a}|$ are in average almost 20 times smaller after introducing the drift compensation component, the average value of an orientation error $\|e_o\|$ slightly increases. This result is also caused by the introduced modification of the VFO controller - to compensate the transversal drift, the vehicle is oriented with a certain inclination to the path and goes partially sideways. The use of the VFO-ADR controller with the transversal drift compensation resulted in the decrease of v_c and τ fluctuations, and the decrease of maximal commanded velocities v_c resulting in lower control signals τ . According to the control objective (21), the terminal upper bound of the control error obtained in the simulation has got the value $\sup_{t \in [90, 100]} \|e_{2\pi}(t)\| \leq \varepsilon_\eta \approx 0.6034$, while the terminal upper bound of position error is approximately equal to $\sup_{t \in [90, 100]} \|e_p(t)\| \leq \varepsilon_p \approx 0.0135$ m.

6. Conclusions

The proposed VFO-ADR control system solves the path-following task for the underactuated torpedo-like vehicles maintaining non-banked motion. Expected characteristics of the derived controller applied to the highly uncertain vehicle model were shown along with the ISS analysis and had been confirmed with the presented simulation study.

The use of an error-based ESO utilized in the ADR controller resulted in the desired output-feedback characteristics of the proposed solution. Presented simulation results have

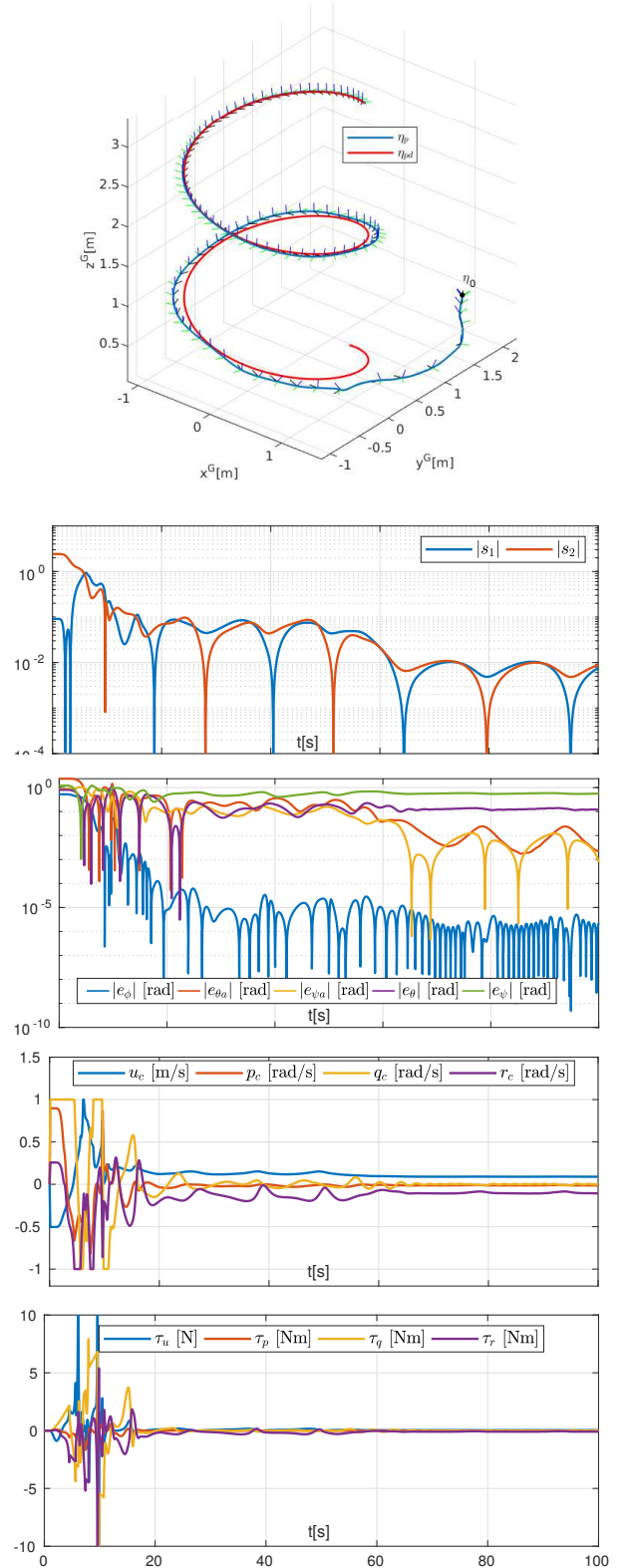


Figure 3: Simulation results for the underactuated rigid body following a helix-like path

shown that the application of a drift compensation component in the VFO controller substantially improves the positional

path-following performance and decrease both fluctuation intensity and maximal amplitudes of control signals.

Using the non-parametrized path definition, we have omitted the need of calculating the distance between the vehicle and the path. The price that needed to be paid for eliminating this appeared in the additional assumptions concerning gradients and Hessians of the level-surface equations, which however do not influence the realtime performance of the control algorithm in the case when a proper reference path is given *a priori*.

Appendix A. Derivation of some path-related quantities

The nominal values of the level surface derivatives can be expressed, upon (23) and (25), as

$$\hat{s}_j = \nabla^\top s_j \hat{\eta}_p = \nabla^\top s_j (\hat{\eta}_{pc} - \hat{\epsilon}_p). \quad (\text{A.1})$$

According to the desired output-feedback characteristics of the VFO-ADR control structure, we propose to use the modified versions of level surface derivatives that are dependent only on the measurable signals, i.e.,

$$\hat{\hat{s}}_j = \nabla^\top s_j (\hat{\eta}_{pc} - \hat{\epsilon}_p). \quad (\text{A.2})$$

The nominal of $\hat{\boldsymbol{\vartheta}}_j$ and $\hat{\boldsymbol{\vartheta}}_\perp$ are described by

$$\hat{\boldsymbol{\vartheta}}_\perp = \sigma \frac{\hat{\boldsymbol{w}}_\perp \boldsymbol{w}_\perp^\top \boldsymbol{w}_\perp - \boldsymbol{w}_\perp \boldsymbol{w}_\perp^\top \hat{\boldsymbol{w}}_\perp}{\|\boldsymbol{w}_\perp\|^3}, \quad (\text{A.3})$$

$$\hat{\boldsymbol{\vartheta}}_j = \frac{-\frac{d}{dt} \nabla s_j \|\nabla s_j\| + \nabla s_j \frac{d}{dt} \|\nabla s_j\|}{\|\nabla s_j\|^2}, \quad (\text{A.4})$$

where $\boldsymbol{w}_\perp \triangleq \nabla s_1 \times \nabla s_2$, and

$$\hat{\boldsymbol{w}}_\perp = \frac{d}{dt} \nabla s_1 \times \nabla s_2 + \nabla s_1 \times \frac{d}{dt} \nabla s_2, \quad (\text{A.5})$$

$$\frac{d}{dt} \nabla s_j = \nabla(\nabla^\top s_j) \hat{\eta}_p \stackrel{(25)}{=} \nabla(\nabla^\top s_j) (\hat{\eta}_{pc} - \hat{\epsilon}_p), \quad (\text{A.6})$$

$$\frac{d}{dt} \|\nabla s_j\| = \frac{\nabla^\top s_j \nabla(\nabla^\top s_j)}{\|\nabla s_j\|} \hat{\eta}_p \stackrel{(25)}{=} \frac{\nabla^\top s_j \nabla(\nabla^\top s_j)}{\|\nabla s_j\|} (\hat{\eta}_{pc} - \hat{\epsilon}_p), \quad (\text{A.7})$$

for $j \in \{1, 2\}$. Analogously to the procedure utilized to transform (A.1) into (A.2), the modified versions of (A.3) and (A.4) have the following form:

$$\hat{\hat{\boldsymbol{\vartheta}}}_\perp = \sigma \frac{\hat{\hat{\boldsymbol{w}}}_\perp \boldsymbol{w}_\perp^\top \boldsymbol{w}_\perp - \boldsymbol{w}_\perp \boldsymbol{w}_\perp^\top \hat{\hat{\boldsymbol{w}}}_\perp}{\|\boldsymbol{w}_\perp\|^3}, \quad (\text{A.8})$$

$$\hat{\hat{\boldsymbol{\vartheta}}}_j = \frac{-\frac{d}{dt} \widehat{\nabla s_j} \|\widehat{\nabla s_j}\| + \widehat{\nabla s_j} \frac{d}{dt} \|\widehat{\nabla s_j}\|}{\|\widehat{\nabla s_j}\|^2}, \quad (\text{A.9})$$

where

$$\hat{\hat{\boldsymbol{w}}}_\perp = \frac{d}{dt} \widehat{\nabla s_1} \times \widehat{\nabla s_2} + \widehat{\nabla s_1} \times \frac{d}{dt} \widehat{\nabla s_2}, \quad (\text{A.10})$$

$$\frac{d}{dt} \widehat{\nabla s_j} = \nabla(\nabla^\top s_j) (\hat{\eta}_{pc} - \hat{\epsilon}_p), \quad (\text{A.11})$$

$$\frac{d}{dt} \|\widehat{\nabla s_j}\| = \frac{\nabla^\top s_j \nabla(\nabla^\top s_j)}{\|\widehat{\nabla s_j}\|} (\hat{\eta}_{pc} - \hat{\epsilon}_p), \quad (\text{A.12})$$

for $j \in \{1, 2\}$.

Appendix B. Velocity error dynamics

Transformations between the velocity dynamics introduced firstly in (26), and the form represented by (66) are based on the mutual relations between particular matrices and vectors utilized in the rigid body dynamics equations in frames $\{B\}$ and $\{G\}$ (see (7), (6)), the form of a modified disturbance vector introduced in (64), and are explained as follows:

$$\dot{\epsilon} \stackrel{(26)}{=} \boldsymbol{d} - \boldsymbol{J} \hat{\boldsymbol{B}} \boldsymbol{\Gamma} \boldsymbol{J}^\top \boldsymbol{\tau}_\eta \quad (\text{B.1})$$

$$= \boldsymbol{d} - \boldsymbol{J} \hat{\boldsymbol{B}} \boldsymbol{\Gamma} \hat{\boldsymbol{B}}^{-1} \boldsymbol{J}^{-1} [\hat{\boldsymbol{d}} + \boldsymbol{K}_\eta \hat{\epsilon}]$$

$$= \boldsymbol{J} \boldsymbol{J}^{-1} \boldsymbol{d} - \boldsymbol{J} \boldsymbol{\Gamma} \boldsymbol{J}^{-1} [\hat{\boldsymbol{d}} + \boldsymbol{K}_\eta \hat{\epsilon}]$$

$$= -\boldsymbol{J} \boldsymbol{\Gamma} \boldsymbol{K} \boldsymbol{J}^{-1} \boldsymbol{\epsilon} + \boldsymbol{J} \boldsymbol{\Gamma} \boldsymbol{K} \boldsymbol{J}^{-1} \tilde{\boldsymbol{\epsilon}} + \boldsymbol{J} \boldsymbol{\Gamma} \boldsymbol{J}^{-1} \tilde{\boldsymbol{d}}$$

$$+ \boldsymbol{J} (\boldsymbol{I} - \boldsymbol{\Gamma}) \boldsymbol{J}^{-1} \boldsymbol{d}$$

$$\stackrel{(64)}{=} -\boldsymbol{J} \boldsymbol{\Gamma} \boldsymbol{K} \boldsymbol{J}^{-1} \boldsymbol{\epsilon} + \boldsymbol{J} \boldsymbol{\Gamma} \boldsymbol{K} \boldsymbol{J}^{-1} \tilde{\boldsymbol{\epsilon}} + \boldsymbol{J} \boldsymbol{\Gamma} \boldsymbol{J}^{-1} \tilde{\boldsymbol{d}}$$

$$+ \boldsymbol{J} (\boldsymbol{I} - \boldsymbol{\Gamma}) \boldsymbol{J}^{-1} [\boldsymbol{d}^* - \boldsymbol{M}_\eta^{-1} \Delta_\eta \boldsymbol{\epsilon}]$$

$$= -\boldsymbol{J} \boldsymbol{\Gamma} \boldsymbol{K} \boldsymbol{J}^{-1} \boldsymbol{\epsilon} + \boldsymbol{J} \boldsymbol{\Gamma} \boldsymbol{K} \boldsymbol{J}^{-1} \tilde{\boldsymbol{\epsilon}} + \boldsymbol{J} \boldsymbol{\Gamma} \boldsymbol{J}^{-1} \tilde{\boldsymbol{d}}$$

$$+ \boldsymbol{J} (\boldsymbol{I} - \boldsymbol{\Gamma}) \boldsymbol{J}^{-1} \boldsymbol{d}^* - \boldsymbol{J} (\boldsymbol{I} - \boldsymbol{\Gamma}) \boldsymbol{M}^{-1} \Delta \boldsymbol{J}^{-1} \boldsymbol{\epsilon}$$

$$= -\boldsymbol{J} (\boldsymbol{\Gamma} \boldsymbol{K} + (\boldsymbol{I} - \boldsymbol{\Gamma}) \boldsymbol{M}^{-1} \Delta) \boldsymbol{J}^{-1} \boldsymbol{\epsilon} + \boldsymbol{J} \boldsymbol{\Gamma} \boldsymbol{K} \boldsymbol{J}^{-1} \tilde{\boldsymbol{\epsilon}}$$

$$+ \boldsymbol{J} \boldsymbol{\Gamma} \boldsymbol{J}^{-1} \tilde{\boldsymbol{d}} + \boldsymbol{J} (\boldsymbol{I} - \boldsymbol{\Gamma}) \boldsymbol{J}^{-1} \boldsymbol{d}^*, \quad (\text{B.2})$$

where $\boldsymbol{K} = \boldsymbol{J}^{-1} \boldsymbol{K}_\eta \boldsymbol{J} \triangleq \text{diag}\{k_1, \dots, k_6\}$ is the ADR controller gain matrix in the local reference frame.

Appendix C. Derivation of $\tilde{\boldsymbol{\eta}}_{oa}$

To calculate the upper-bound of the $\tilde{\boldsymbol{\eta}}_{oa}$, introduced in (68), the error between the nominal and approximated longitudinal convergence vector field derivatives

$$\tilde{\boldsymbol{h}}_p^* = [\tilde{\hat{h}}_x^* \tilde{\hat{h}}_x^* \tilde{\hat{h}}_z^*]^\top \triangleq \hat{\boldsymbol{h}}_p^* - \hat{\hat{\boldsymbol{h}}}_p^* \quad (\text{C.1})$$

have to be determined and evaluated. Based on the equations (56) and (58), we can write down that

$$\tilde{\boldsymbol{h}}_p^* = u_d \tilde{\boldsymbol{\vartheta}}_\perp + \tilde{s}_1 \boldsymbol{\vartheta}_1 + s_1 \tilde{\boldsymbol{\vartheta}}_1 + \tilde{s}_2 \boldsymbol{\vartheta}_2 + s_2 \tilde{\boldsymbol{\vartheta}}_2 \quad (\text{C.2})$$

where $\tilde{\boldsymbol{\vartheta}}_\perp \triangleq \hat{\boldsymbol{\vartheta}}_\perp - \hat{\hat{\boldsymbol{\vartheta}}}_\perp$, $\tilde{\boldsymbol{\vartheta}}_j \triangleq \hat{\boldsymbol{\vartheta}}_j - \hat{\hat{\boldsymbol{\vartheta}}}_j$, and $\tilde{s}_j \triangleq \hat{s}_j - \hat{\hat{s}}_j$ for $j \in \{1, 2\}$. Then, according to the derivations presented in the Appendix A, we know that

$$\tilde{s}_j = \hat{s}_j - \hat{\hat{s}}_j = \nabla^\top s_j (\hat{\epsilon}_p - \epsilon_p) = \nabla^\top s_j \tilde{\boldsymbol{\epsilon}}_p, \quad (\text{C.3})$$

$$\tilde{\boldsymbol{\vartheta}}_\perp = \sigma \frac{\tilde{\boldsymbol{w}}_\perp \boldsymbol{w}_\perp^\top \boldsymbol{w}_\perp - \boldsymbol{w}_\perp \boldsymbol{w}_\perp^\top \tilde{\boldsymbol{w}}_\perp}{\|\boldsymbol{w}_\perp\|^3}, \quad (\text{C.4})$$

$$\tilde{\boldsymbol{\vartheta}}_j = \frac{-\frac{d}{dt} \widetilde{\nabla s_j} \|\widetilde{\nabla s_j}\| + \widetilde{\nabla s_j} \frac{d}{dt} \|\widetilde{\nabla s_j}\|}{\|\widetilde{\nabla s_j}\|^2}, \quad (\text{C.5})$$

where

$$\tilde{\mathbf{w}}_{\perp} \triangleq \hat{\mathbf{w}}_{\perp} - \hat{\mathbf{w}}_{\perp} \stackrel{(A.10)}{=} \widetilde{\frac{d}{dt} \nabla s_1 \times \nabla s_2 + \nabla s_1 \times \frac{d}{dt} \nabla s_2}, \quad (C.6)$$

$$\widetilde{\frac{d}{dt} \nabla s_j} \triangleq \frac{d}{dt} \nabla s_j - \frac{d}{dt} \widehat{\nabla s_j} = \nabla(\nabla^{\top} s_j) \tilde{\boldsymbol{\epsilon}}_p, \quad (C.7)$$

$$\frac{d}{dt} \|\nabla s_j\| \triangleq \frac{d}{dt} \|\nabla s_j\| - \frac{d}{dt} \widehat{\|\nabla s_j\|} = \frac{\nabla^{\top} s_j \nabla(\nabla^{\top} s_j)}{\|\nabla s_j\|} \tilde{\boldsymbol{\epsilon}}_p. \quad (C.8)$$

Upon the above forms and Assumptions 5 and 6, we can obtain the following set of conservative bounds

$$\|\tilde{s}_j\| \leq \|\nabla s_j\| \|\tilde{\boldsymbol{\epsilon}}_p\| \leq \bar{m}_j \|\tilde{\boldsymbol{\chi}}\|, \quad (C.9)$$

$$\|\widetilde{\frac{d}{dt} \nabla s_j}\| \leq \|\nabla(\nabla^{\top} s_j)\| \|\tilde{\boldsymbol{\epsilon}}_p\| \leq \bar{M}_j \|\tilde{\boldsymbol{\chi}}\|, \quad (C.10)$$

$$\|\frac{d}{dt} \|\nabla s_j\|\| \leq \frac{\|\nabla s_j\| \|\nabla(\nabla^{\top} s_j)\|}{\|\nabla s_j\|} \|\tilde{\boldsymbol{\epsilon}}_p\| \leq \bar{M}_j \|\tilde{\boldsymbol{\chi}}\|, \quad (C.11)$$

$$\|\tilde{\mathbf{w}}_{\perp}\| \leq (\bar{M}_1 \bar{m}_2 + \bar{m}_1 \bar{M}_2) \|\tilde{\boldsymbol{\chi}}\|, \quad (C.12)$$

$$\|\mathbf{w}_{\perp}\| \geq \underline{m}_1 \underline{m}_2, \quad (C.13)$$

$$\|\tilde{\boldsymbol{\theta}}_{\perp}\| \leq \frac{2(\bar{M}_1 \bar{m}_2 + \bar{m}_1 \bar{M}_2)}{\underline{m}_1 \underline{m}_2} \|\tilde{\boldsymbol{\chi}}\|, \quad (C.14)$$

$$\|\tilde{\boldsymbol{\theta}}_j\| \leq \frac{2\bar{M}_j}{\underline{m}_j} \|\tilde{\boldsymbol{\chi}}\|, \quad (C.15)$$

and determine the upper bound function of the estimation error of the convergence vector field derivative

$$\|\tilde{\hat{\mathbf{h}}}_p^*\| \leq |f_h| \|\tilde{\boldsymbol{\chi}}\|, \quad (C.16)$$

with

$$|f_h| = |u_d| \frac{2(\bar{M}_1 \bar{m}_2 + \bar{m}_1 \bar{M}_2)}{\underline{m}_1 \underline{m}_2} + (\bar{m}_1 + \bar{m}_2) + \frac{2\bar{M}_1}{\underline{m}_1} |s_1| + \frac{2\bar{M}_2}{\underline{m}_2} |s_2|. \quad (C.17)$$

Now, having in mind the result (C.16), an analysis of particular auxiliary angle derivative errors can be written down as

$$\tilde{\psi}_a = \frac{\tilde{\hat{h}}_y^* \hat{h}_x^* - \tilde{\hat{h}}_x^* \hat{h}_y^*}{\hat{h}_x^{*2} + \hat{h}_y^{*2}}, \quad (C.18)$$

$$\tilde{\theta}_a = \frac{-\beta_6}{\hat{h}_z^{*2} + (\hat{h}_x^* c\psi_a + \hat{h}_y^* s\psi_a)^2}, \quad (C.19)$$

where

$$\beta_6 = [\hat{h}_z^* (\hat{h}_x^* c\psi_a + \hat{h}_y^* s\psi_a) - \hat{h}_z^* (\tilde{\hat{h}}_x^* c\psi_a + \tilde{\hat{h}}_y^* s\psi_a - \hat{h}_x^* \tilde{\psi}_a s\psi_a + \hat{h}_y^* \tilde{\psi}_a c\psi_a)]. \quad (C.20)$$

The absolute values of the $\tilde{\boldsymbol{\eta}}_{oa}$ elements can be then estimated

as

$$|\tilde{\psi}_a| \leq \underbrace{\frac{|\hat{h}_x^*| + |\hat{h}_y^*|}{\hat{h}_x^{*2} + \hat{h}_y^{*2}}}_{|f_{\psi}|} \|\tilde{\hat{\mathbf{h}}}_p\| \leq |f_{\psi}| |f_h| \|\tilde{\boldsymbol{\chi}}\|, \quad (C.21)$$

$$|\tilde{\theta}_a| \leq |f_{\theta}| \|\tilde{\hat{\mathbf{h}}}_p\| \leq |f_{\theta}| |f_h| \|\tilde{\boldsymbol{\chi}}\|, \quad (C.22)$$

where

$$|f_{\theta}| = \frac{|\hat{h}_x^*| + |\hat{h}_y^*| + 2|\hat{h}_z^*| + |\hat{h}_z^*| (|\hat{h}_x^*| + |\hat{h}_y^*|) |f_{\psi}|}{\hat{h}_z^{*2} + (\hat{h}_x^* c\psi_a + \hat{h}_y^* s\psi_a)^2}. \quad (C.23)$$

Now, the upper bound of the auxiliary angle derivative error

$$\|\tilde{\boldsymbol{\eta}}_{oa}(t)\| \leq \sup_{t \geq 0} (|f_{\psi}(t)| |f_h(t)| + |f_{\theta}(t)| |f_h(t)|) \|\tilde{\boldsymbol{\chi}}(t)\|. \quad (C.24)$$

Since the analysis provided in this article is assumed to be valid locally and we assume that the initial conditions of any vector are in some compact set (see Remark 9), the expression $\sup_{t \geq 0} (|f_{\psi}(t)| |f_h(t)| + |f_{\theta}(t)| |f_h(t)|)$ is finite.

Appendix D. Estimation of the \dot{V}_p

According to the definition of the Lyapunov function for the position error dynamics (113), and upon dynamics (71) and (72), a derivative of the Lyapunov function can be written down as

$$\begin{aligned} \dot{V}_p &= \frac{1}{\|\nabla s_1\|} s_1 \dot{s}_1 + \frac{1}{\|\nabla s_2\|} s_2 \dot{s}_2 \\ &= (s_1 \boldsymbol{\theta}_1^{\top} + s_2 \boldsymbol{\theta}_2^{\top}) (\dot{\boldsymbol{\eta}}_{pc} - \boldsymbol{\epsilon}_p - \hat{\mathbf{h}}_p^* + \delta_p \tilde{\boldsymbol{\epsilon}}_p) \\ &\quad - k_p \mathbf{e}_p^{\top} \underbrace{\begin{bmatrix} 1 & c\kappa \\ c\kappa & 1 \end{bmatrix}}_{\mathbf{H}_p} \mathbf{e}_p \\ &= -k_p \mathbf{e}_p^{\top} \mathbf{H}_p \mathbf{e}_p - \mathbf{e}_p^{\top} \begin{bmatrix} \boldsymbol{\theta}_1^{\top} \\ \boldsymbol{\theta}_2^{\top} \end{bmatrix} \mathbf{r} - \mathbf{e}_p^{\top} \begin{bmatrix} \boldsymbol{\theta}_1^{\top} \\ \boldsymbol{\theta}_2^{\top} \end{bmatrix} ((1 - \delta_p) \boldsymbol{\epsilon}_p + \delta_p \tilde{\boldsymbol{\epsilon}}_p), \end{aligned} \quad (D.1)$$

where $\kappa \angle (\nabla s_1, \nabla s_2) \neq k\pi$, $k \in \mathbb{Z}$ correspond to the angle between the level-surface gradients with the values constrained according to the Assumption 7, and the residual vector

$$\mathbf{r} \triangleq \hat{\mathbf{h}}_p^* - \dot{\boldsymbol{\eta}}_{pc} = \hat{\mathbf{h}}_p^* - \mathbf{R} \mathbf{v}_{pc} = \hat{\mathbf{h}}_p^* - u_c \boldsymbol{\gamma}, \quad (D.2)$$

for

$$\boldsymbol{\gamma} \triangleq [c\theta c\psi \quad c\theta s\psi \quad -s\theta]^{\top}, \quad \|\boldsymbol{\gamma}\| = 1. \quad (D.3)$$

Referring to the equation (61), we can express the residual vector from (D.2) as

$$\mathbf{r} = \|\hat{\mathbf{h}}_p^*\| \left(\begin{bmatrix} \frac{\hat{h}_x^*}{\|\hat{\mathbf{h}}_p^*\|} \\ \frac{\hat{h}_y^*}{\|\hat{\mathbf{h}}_p^*\|} \\ \frac{\hat{h}_z^*}{\|\hat{\mathbf{h}}_p^*\|} \end{bmatrix} - \begin{bmatrix} c\theta c\psi \\ c\theta s\psi \\ -c\theta \end{bmatrix} \right), \quad (D.4)$$

where $\alpha = \angle(\hat{\mathbf{h}}_p^*, \boldsymbol{\gamma})$, and write down that

$$\begin{aligned}
\|\mathbf{r}\|^2 &= \|\hat{\mathbf{h}}_p^*\|^2 \left[\frac{\hat{h}_x^2}{\|\hat{\mathbf{h}}_p^*\|^2} - \frac{2\hat{h}_x^*}{\|\hat{\mathbf{h}}_p^*\|} c\alpha c\theta c\psi + c^2\alpha c^2\theta c^2\psi \right. \\
&\quad + \frac{\hat{h}_y^2}{\|\hat{\mathbf{h}}_p^*\|^2} - \frac{2\hat{h}_y^*}{\|\hat{\mathbf{h}}_p^*\|} c\alpha c\theta s\psi + c^2\alpha c^2\theta s^2\psi \\
&\quad \left. + \frac{\hat{h}_z^2}{\|\hat{\mathbf{h}}_p^*\|^2} + \frac{2\hat{h}_z^*}{\|\hat{\mathbf{h}}_p^*\|} c\alpha s\theta + c^2\alpha s^2\theta \right] \\
&= \|\hat{\mathbf{h}}_p^*\|^2 \left[1 - 2c\alpha \underbrace{\frac{\hat{h}_x^* c\theta c\psi + \hat{h}_y^* c\theta s\psi - \hat{h}_z^* s\theta}{\|\hat{\mathbf{h}}_p^*\|}}_{c\alpha} + c^2\alpha \right] \\
&= \|\hat{\mathbf{h}}_p^*\|^2 (1 - c^2\alpha). \tag{D.5}
\end{aligned}$$

Using the interpretation of auxiliary angles θ_a and ψ_a defined in (49), the longitudinal part of the modified convergence vector field can be rewritten as

$$\hat{\mathbf{h}}_p^* = \|\hat{\mathbf{h}}_p^*\| \begin{bmatrix} \xi_d c\theta_a c\psi_a \\ \xi_d c\theta_a s\psi_a \\ -\xi_d s\theta_a \end{bmatrix}, \tag{D.6}$$

and

$$\begin{aligned}
c\alpha &= \frac{\hat{\mathbf{h}}_p^{*\top} \boldsymbol{\gamma}}{\|\hat{\mathbf{h}}_p^*\| \|\boldsymbol{\gamma}\|} = \begin{bmatrix} \xi_d c\theta_a c\psi_a & \xi_d c\theta_a s\psi_a & -\xi_d s\theta_a \end{bmatrix} \begin{bmatrix} c\theta c\psi \\ c\theta s\psi \\ -s\theta \end{bmatrix} \\
&= \xi_d c\theta_a c\psi_a c\theta c\psi + \xi_d c\theta_a s\psi_a c\theta s\psi + \xi_d s\theta_a s\theta \\
&= \xi_d c\theta_a c\theta (c\psi_a c\psi + s\psi_a s\psi) + \xi_d s\theta_a s\theta \\
&= \xi_d c\theta_a c\theta c e_{\psi_a} + \xi_d s\theta_a s\theta. \tag{D.7}
\end{aligned}$$

Using the trygonometric identities

$$c\theta = c(\theta_a - e_{\theta_a}) = c\theta_a c e_{\theta_a} + s\theta_a s e_{\theta_a} \tag{D.8}$$

$$s\theta = s(\theta_a - e_{\theta_a}) = s\theta_a c e_{\theta_a} - c\theta_a s e_{\theta_a} \tag{D.9}$$

$$c\psi = c(\psi_a - e_{\psi_a}) = c\psi_a c e_{\psi_a} + s\psi_a s e_{\psi_a} \tag{D.10}$$

$$s\psi = s(\psi_a - e_{\psi_a}) = s\psi_a c e_{\psi_a} - c\psi_a s e_{\psi_a} \tag{D.11}$$

$$(1 - c e_{\psi_a}) = 2s^2 \frac{e_{\psi_a}}{2}, \tag{D.12}$$

together with the equivalence

$$1 \equiv (s^2\theta_a + c^2\theta_a)^2 (c^2 e_{\theta_a} c^2 e_{\psi_a} + c^2 e_{\theta_a} s^2 e_{\psi_a} + s^2 e_{\theta_a}), \tag{D.13}$$

after some algebraic transformations, we can write down that

$$\begin{aligned}
1 - c^2\alpha &= 1 - \left[c^2\theta_a c^2\theta c^2 e_{\psi_a} + 2c\theta_a c\theta c e_{\psi_a} s\theta_a s\theta + s^2\theta_a s^2\theta \right] \\
&= -s^4\theta_a c^2 e_{\theta_a} s^2 e_{\psi_a} + s^4\theta_a c^2 e_{\theta_a} s^2 e_{\psi_a} \\
&\quad + s^2 e_{\theta_a} (s^4\theta_a + c^4\theta_a) - 4s^2\theta_a c^2\theta_a c^2 e_{\theta_a} s^2 \frac{e_{\psi_a}}{2} c e_{\psi_a} \\
&\quad + 2s^2\theta_a c^2\theta_a c^2 e_{\theta_a} s^2 e_{\psi_a} \\
&\quad + 2c^2\theta_a s^2\theta_a s^2 e_{\theta_a} (1 + c e_{\psi_a}) + c^4\theta_a c^2 e_{\theta_a} s^2 e_{\psi_a} \\
&\quad + 4c\theta_a s\theta_a c e_{\theta_a} s e_{\theta_a} s^2 \frac{e_{\psi_a}}{2} (c^2\theta_a c e_{\psi_a} + s^2\theta_a) \\
&\quad - c^2\theta_a s^2\theta_a s^2 e_{\theta_a} (1 + c^2 e_{\psi_a}). \tag{D.14}
\end{aligned}$$

Knowing that $|c\rho| \leq 1$, $|s\rho| \leq 1$, and $|s\rho| \leq |\rho|$, an upper bound of the expression (D.14) can be (conservatively) assessed as follows

$$\begin{aligned}
|1 - c^2\alpha| &\leq 7|e_{\theta_a}|^2 + 5|e_{\psi_a}|^2 \\
&= \begin{bmatrix} e_{\theta_a} & e_{\psi_a} \end{bmatrix} \begin{bmatrix} 7 & 0 \\ 0 & 5 \end{bmatrix} \begin{bmatrix} e_{\theta_a} \\ e_{\psi_a} \end{bmatrix} \\
&= \bar{\mathbf{e}}_a \mathbf{H}_\alpha \bar{\mathbf{e}}_a \leq \lambda_{\max}(\mathbf{H}_\alpha) \|\bar{\mathbf{e}}_a\|^2 = 7\|\bar{\mathbf{e}}_a\|^2, \tag{D.15}
\end{aligned}$$

implying that

$$\sqrt{1 - c^2\alpha} = \sqrt{|1 - c^2\alpha|} \leq \sqrt{7\|\bar{\mathbf{e}}_a\|^2} = \sqrt{7}\|\bar{\mathbf{e}}_a\|. \tag{D.16}$$

The upper bound function of the longitudinal modified convergence vector field estimate, according to (44), (45), and (62), may be written down in the form

$$\|\hat{\mathbf{h}}_p^*\| \leq |u_d| + k_p \|\mathbf{e}_p\| + \delta_p (\|\boldsymbol{\epsilon}_p\| + \|\tilde{\boldsymbol{\epsilon}}_p\|). \tag{D.17}$$

According to the results (D.5), (D.15), and (D.17), we can say that the derivative of V_p is bounded by

$$\begin{aligned}
\dot{V}_p &= -k_p \mathbf{e}_p^\top \mathbf{H}_p \mathbf{e}_p - \mathbf{e}_p^\top \begin{bmatrix} \boldsymbol{\vartheta}_1^\top \\ \boldsymbol{\vartheta}_2^\top \end{bmatrix} \mathbf{r} - \mathbf{e}_p^\top \begin{bmatrix} \boldsymbol{\vartheta}_1^\top \\ \boldsymbol{\vartheta}_2^\top \end{bmatrix} \left((1 - \delta_p) \boldsymbol{\epsilon}_p + \delta_p \tilde{\boldsymbol{\epsilon}}_p \right) \\
&\leq -k_p \mathbf{e}_p^\top \mathbf{H}_p \mathbf{e}_p + 2\|\mathbf{e}_p\| (\|\mathbf{r}\| + (1 - \delta_p) \|\boldsymbol{\epsilon}_p\| + \delta_p \|\tilde{\boldsymbol{\epsilon}}_p\|) \\
&\leq -k_p (1 - \nu_p) \mathbf{e}_p^\top \mathbf{H}_p \mathbf{e}_p + \|\mathbf{e}_p\| \left[2(1 - \delta_p) \|\boldsymbol{\epsilon}_p\| \right. \\
&\quad \left. + 2\delta_p \|\tilde{\boldsymbol{\epsilon}}_p\| + 2\sqrt{7}|u_d| \|\bar{\mathbf{e}}_a\| + 2\sqrt{7}\delta_p (\|\boldsymbol{\epsilon}_p\| + \|\tilde{\boldsymbol{\epsilon}}_p\|) \|\bar{\mathbf{e}}_a\| \right. \\
&\quad \left. - k_p \|\mathbf{e}_p\| (\lambda_{\min}(\mathbf{H}_p) \nu_p - 2\sqrt{7}\|\bar{\mathbf{e}}_a\|) \right]. \tag{D.18}
\end{aligned}$$

Appendix E. Difference between the desired and auxiliary yaw angles

The transformation from (132) into (133), was done using the relation

$$\text{Atan2}(Y_1, X_1) - \text{Atan2}(Y_2, X_2) = \text{Atan2}(\rho_6, \rho_7), \tag{E.1}$$

where $\rho_6 := Y_1 X_2 - Y_2 X_1$, and $\rho_7 := X_1 X_2 + Y_1 Y_2$. Subsequent transformation can be explained as follows:

$$\begin{aligned}
\varepsilon_\psi &\triangleq \psi_d - \psi_a^* = \psi_d - \text{Atan2}(s\psi_a, c\psi_a) \\
&= \text{Atan2}(\xi_d \vartheta_{\perp y}, \xi_d \vartheta_{\perp x}) - \text{Atan2}(\xi_d \hat{h}_y^*, \xi_d \hat{h}_x^*) \\
&= \text{Atan2}(\hat{h}_x^* \vartheta_{\perp y} - \hat{h}_y^* \vartheta_{\perp x}, \hat{h}_x^* \vartheta_{\perp x} + \hat{h}_y^* \vartheta_{\perp y}) \\
&\stackrel{(44)}{=} \text{Atan2}(-k_p s_1 [\vartheta_{1x} \vartheta_{\perp y} - \vartheta_{1y} \vartheta_{\perp x}] \\
&\quad - k_p s_2 [\vartheta_{2x} \vartheta_{\perp y} - \vartheta_{2y} \vartheta_{\perp x}] + \delta_p (\hat{\mathbf{e}}_1 \vartheta_{\perp x} - \hat{\mathbf{e}}_2 \vartheta_{\perp y}), \\
&\quad u_d [\vartheta_{\perp x}^2 + \vartheta_{\perp y}^2] - k_p s_1 [\vartheta_{\perp y} \vartheta_{1y} + \vartheta_{\perp x} \vartheta_{1x}] \\
&\quad - k_p s_2 [\vartheta_{\perp x} \vartheta_{2x} + \vartheta_{\perp y} \vartheta_{2y}] + \delta_p (\hat{\mathbf{e}}_1 \vartheta_{\perp x} + \hat{\mathbf{e}}_2 \vartheta_{\perp y})) \\
&= \text{Atan2}(-k_p s_1 \bar{\boldsymbol{\vartheta}}_1 \otimes \bar{\boldsymbol{\vartheta}}_{\perp} - k_p s_2 \bar{\boldsymbol{\vartheta}}_2 \otimes \bar{\boldsymbol{\vartheta}}_{\perp} \\
&\quad + \delta_p (\hat{\mathbf{e}}_1 \vartheta_{\perp x} - \hat{\mathbf{e}}_2 \vartheta_{\perp y}), \\
&\quad u_d \bar{\boldsymbol{\vartheta}}_{\perp}^{\top} \bar{\boldsymbol{\vartheta}}_{\perp} - k_p s_1 \bar{\boldsymbol{\vartheta}}_1^{\top} \bar{\boldsymbol{\vartheta}}_{\perp} - k_p s_2 \bar{\boldsymbol{\vartheta}}_2^{\top} \bar{\boldsymbol{\vartheta}}_{\perp} + \delta_p \hat{\boldsymbol{\epsilon}}_p^{\top} \bar{\boldsymbol{\vartheta}}_{\perp}), \tag{E.2}
\end{aligned}$$

where $\bar{\boldsymbol{\vartheta}}_i \triangleq [\vartheta_{ix} \ \vartheta_{iy}]^\top$ for $i \in \{1, 2\}$, and $\bar{\boldsymbol{\vartheta}}_{\perp} \triangleq [\vartheta_{\perp x} \ \vartheta_{\perp y}]^\top$, while the operation $\mathbf{a} \otimes \mathbf{b} \triangleq a_1 b_2 - a_2 b_1$ for some vectors

$\mathbf{a} = [a_1 \ a_2]^\top \in \mathbb{R}^2$ and $\mathbf{b} = [b_1 \ b_2]^\top \in \mathbb{R}^2$. The upper-bound function of the absolute value of (E.2) can be expressed as

$$\begin{aligned} |\varepsilon_\psi| &\leq \text{Atan2}(k_p \|e_p\| \|\bar{\boldsymbol{\vartheta}}_1\| \|\bar{\boldsymbol{\vartheta}}_\perp\| s\beta_1 + k_p \|e_p\| \|\bar{\boldsymbol{\vartheta}}_2\| \|\bar{\boldsymbol{\vartheta}}_\perp\| s\beta_2) \\ &\quad + \delta_p \|\hat{\boldsymbol{\epsilon}}_p\| \|\bar{\boldsymbol{\vartheta}}_\perp\|, \\ &\quad \left| u_d \|\bar{\boldsymbol{\vartheta}}_\perp\|^2 - k_p s_1 \bar{\boldsymbol{\vartheta}}_1^\top \bar{\boldsymbol{\vartheta}}_\perp - k_p s_2 \bar{\boldsymbol{\vartheta}}_2^\top \bar{\boldsymbol{\vartheta}}_\perp + \delta_p \hat{\boldsymbol{\epsilon}}_o^\top \bar{\boldsymbol{\vartheta}}_\perp \right| \\ &\leq \text{Atan2}(2k_p \|e_p\| + \delta_p \|\boldsymbol{\epsilon}_p\| + \delta_p \|\bar{\boldsymbol{\epsilon}}_p\|, \\ &\quad \left| u_d \|\bar{\boldsymbol{\vartheta}}_\perp\|^2 - k_p s_1 \bar{\boldsymbol{\vartheta}}_1^\top \bar{\boldsymbol{\vartheta}}_\perp - k_p s_2 \bar{\boldsymbol{\vartheta}}_2^\top \bar{\boldsymbol{\vartheta}}_\perp + \delta_p \hat{\boldsymbol{\epsilon}}_o^\top \bar{\boldsymbol{\vartheta}}_\perp \right|), \end{aligned} \quad (\text{E.3})$$

where $\beta_i = \angle(\bar{\boldsymbol{\vartheta}}_i, \bar{\boldsymbol{\vartheta}}_\perp)$.

Appendix F. Difference between the desired and auxiliary pitch angles

In order to obtain ε_θ (see (138)), we have used the relationship

$$\arctan(X_1) - \arctan(X_2) = \arctan\left(\frac{X_1 - X_2}{1 + X_1 X_2}\right), \quad (\text{F.1})$$

leading to

$$\begin{aligned} \varepsilon_\theta &\triangleq \theta_d - \theta_a \\ &\stackrel{(16)(49)}{=} \arctan\left(\frac{-\vartheta_{\perp z}}{\vartheta_{\perp x} c\psi_d + \vartheta_{\perp y} s\psi_d}\right) - \arctan\left(\frac{-\hat{h}_z^*}{\hat{h}_x^* c\psi_a + \hat{h}_y^* s\psi_a}\right) \\ &\stackrel{(15)(49)}{=} \arctan\left(\frac{-\xi_d \vartheta_{\perp z}}{\sqrt{\vartheta_{\perp x}^2 + \vartheta_{\perp y}^2}}\right) - \arctan\left(\frac{-\xi_d \hat{h}_z^*}{\sqrt{\hat{h}_x^{*2} + \hat{h}_y^{*2}}}\right) \\ &= \arctan\left(\frac{\xi_d \hat{h}_z^* \sqrt{\vartheta_{\perp x}^2 + \vartheta_{\perp y}^2} - \xi_d \vartheta_{\perp z} \sqrt{\hat{h}_x^{*2} + \hat{h}_y^{*2}}}{\sqrt{\vartheta_{\perp x}^2 + \vartheta_{\perp y}^2} \sqrt{\hat{h}_x^{*2} + \hat{h}_y^{*2}} + \hat{h}_z^* \vartheta_{\perp z}}\right) \\ &= \arctan\left(\frac{\xi_d \hat{h}_z^* \|\bar{\boldsymbol{\vartheta}}_\perp\| - \xi_d \vartheta_{\perp z} \sqrt{\hat{h}_x^{*2} + \hat{h}_y^{*2}}}{\|\bar{\boldsymbol{\vartheta}}_\perp\| \sqrt{\hat{h}_x^{*2} + \hat{h}_y^{*2}} + \hat{h}_z^* \vartheta_{\perp z}}\right). \end{aligned} \quad (\text{F.2})$$

References

References

- [1] A. Abdessameud and A. Tayebi. Global trajectory tracking control of VTOL-UAVs without linear velocity measurements. *Automatica*, 46(6):1053–1059, 2010.
- [2] J. R. Azinheira and A. Moutinho. Hover control of an UAV with backstepping design including input saturations. *IEEE Transactions on Control Systems Technology*, 16(3):517–526, 2008.
- [3] J. R. Azinheira, A. Moutinho, and E. C. de Paiva. A backstepping controller for path-tracking of an underactuated autonomous airship. *International Journal of Robust and Nonlinear Control*, 18(October 2014):557–569, 2008.
- [4] Yuliang Bai, James D. Biggs, Xiaogang Wang, and Naigang Cui. A singular adaptive attitude control with active disturbance rejection. *European Journal of Control*, 35:50 – 56, 2017.
- [5] D. Brescianini and R. D’Andrea. Design, modeling and control of an omni-directional aerial vehicle. In *2016 IEEE International Conference on Robotics and Automation (ICRA)*, pages 3261–3266, May 2016.

- [6] W. Caharija and et al. Integral Line-of-Sight Guidance and Control of Underactuated Marine Vehicles. *IEEE Transactions on control systems technology*, 24(5):1–20, 2014.
- [7] Ely Carneiro de Paiva, José Raul Azinheira, Josué G. Ramos Jr., Alexandra Moutinho, and Samuel Siqueira Bueno. Project aurora: Infrastructure and flight control experiments for a robotic airship. *Journal of Field Robotics*, 23(3-4):201–222, 2006.
- [8] T. I. Fossen. *Guidance and control of ocean vehicles*. John Wiley & Sons, Chichester, 1999.
- [9] Zhiqiang Gao. Active disturbance rejection control: A paradigm shift in feedback control system design. *Proceedings of the American Control Conference*, 2006:2399–2405, 2006.
- [10] James E. Gentle. *Matrix Algebra, Theory, Computations, and Applications in Statistics*. Springer-Verlag New York, 1st edition, 2007.
- [11] C. Guo, Y. Han, H. Yu, and J. Qin. Spatial path-following control of underactuated auv with multiple uncertainties and input saturation. *IEEE Access*, 7:98014–98022, 2019.
- [12] J. Han. From pid to active disturbance rejection control. *IEEE Transactions on Industrial Electronics*, 56(3):900–906, March 2009.
- [13] Yi Huang and Wenchao Xue. Active disturbance rejection control: Methodology and theoretical analysis. *ISA Transactions*, 53(4):963–976, 2014.
- [14] C.P. Bechlioulis i in. Trajectory Tracking with Prescribed Performance for Underactuated Underwater Vehicles under Model Uncertainties and External Disturbances. *IEEE Transactions on Control Systems Technology*, 25(2):429–440, 2017.
- [15] Alberto Isidori. *Stabilization of Multivariable Nonlinear Systems: Part I*, pages 293–317. Springer International Publishing, Cham, 2017.
- [16] Charles R. Johnson and Michael J. Tsatsomeros. Convex sets of nonsingular and p–matrices. *Linear and Multilinear Algebra*, 38(3):233–239, 1995.
- [17] Y. Kang and J. K. Hedrick. Linear tracking for a fixed-wing uav using nonlinear model predictive control. *IEEE Transactions on Control Systems Technology*, 17(5):1202–1210, Sep. 2009.
- [18] H. K. Khalil. *Nonlinear systems, third edition*. Prentice Hall, New Jersey, 2002.
- [19] Hassan K. Khalil and Laurent Praly. High-gain observers in nonlinear feedback control. *International Journal of Robust and Nonlinear Control*, 24(6):993–1015, 2014.
- [20] K. Łakomy and M. M. Michałek. The VFO path-following kinematic controller for robotic vehicles moving in a 3D space. *RoMoCo 2017*, pages 263–268, 2017, Wałowo, Poland.
- [21] K. Łakomy and M. M. Michałek. VFO-ADR path-following controller with transversal-drift compensation for underactuated vehicles moving in a 3D space [In Polish]. *Postępy robotyki, wolumen 196 serii Prace naukowe. Elektronika, K. Tchoń, C. Zieliński, editors*, pages 199–208, 2018.
- [22] K. Łakomy, M. M. Michałek, and W. Adamski. Scaling of commanded signals in a cascade control system addressing velocity and acceleration limitations of robotic uavs. *IFAC-PapersOnLine*, 52(12):73 – 78, 2019. 21st IFAC Symposium on Automatic Control in Aerospace ACA 2019.
- [23] R. Madonski, M. Ramirez-Neria, M. Stanković, S. Shao, Z. Gao, J. Yang, and S. Li. On vibration suppression and trajectory tracking in largely uncertain torsional system: An error-based ADRC approach. *Mechanical Systems and Signal Processing*, 134:106300, 2019.
- [24] Stephen C Martin and Louis L Whitcomb. Fully actuated model-based control with six-degree-of-freedom coupled dynamical plant models for underwater vehicles: Theory and experimental evaluation. *The International Journal of Robotics Research*, 35(10):1164–1184, 2016.
- [25] M. M. Michałek. Robust trajectory following without availability of the reference time-derivatives in the control scheme with active disturbance rejection. *Proceedings of the 2016 American Control Conference*, pages 1536–1541, 2016, Boston, MA, USA.
- [26] M. M. Michałek, P. Dutkiewicz, M. Kielczewski, and D. Pazderski. Vector-Field-Orientation tracking control for a mobile vehicle disturbed by the skid-slip phenomena. *Journal of Intelligent & Robotic Systems*, 3-4(59):341–365, 2010.
- [27] M. M. Michałek and K. Kozłowski. Vector-field-orientation feedback control method for a differentially driven vehicle. *IEEE Transactions on Control Systems Technology*, 18(1):45–65, 2010.
- [28] M. M. Michałek, K. Łakomy, and W. Adamski. Robust output-feedback

- cascaded tracking controller for spatial motion of anisotropically-actuated vehicles. *Aerospace Science and Technology*, 92:915 – 929, 2019.
- [29] Phuong D. Nguyen, Carmine T. Recchiuto, and Antonio Sgorbissa. Real-Time Path Generation and Obstacle Avoidance for Multirotors: A Novel Approach. *Journal of Intelligent and Robotic Systems: Theory and Applications*, 89(1-2):27–49, 2018.
- [30] Z. Peng and J. Wang. Output-feedback path-following control of autonomous underwater vehicles based on an extended state observer and projection neural networks. *IEEE Transactions on Systems, Man, and Cybernetics: Systems*, 48(4):535–544, April 2018.
- [31] Guilherme V. Raffo, Manuel G. Ortega, and Francisco R. Rubio. An integral predictive/nonlinear H_∞ control structure for a quadrotor helicopter. *Automatica*, 46(1):29 – 39, 2010.
- [32] M. F. Reis, R. P. Jain, A. P. Aguiar, and J. B. de Sousa. Robust moving path following control for robotic vehicles: Theory and experiments. *IEEE Robotics and Automation Letters*, 4(4):3192–3199, Oct 2019.
- [33] Antonio Sgorbissa. Integrated robot planning, path following, and obstacle avoidance in two and three dimensions: Wheeled robots, underwater vehicles, and multicopters. *The International Journal of Robotics Research*, 38(7):853–876, 2019.
- [34] Xingling Shao, Linwei Wang, Jie Li, and Jun Liu. High-order ESO based output feedback dynamic surface control for quadrotors under position constraints and uncertainties. *Aerospace Science and Technology*, 89:288 – 298, 2019.
- [35] Yuri Shtessel, Christopher Edwards, Leonid Fridman, and Arie Levant. *Sliding Mode Control and Observation*. Birkhauser Basel, 1st edition, 2015.
- [36] E. D. Sontag and Yuan Wang. New characterizations of input-to-state stability. *IEEE Transactions on Automatic Control*, 41(9):1283–1294, Sep. 1996.
- [37] L. Sun and Z. Zheng. Nonlinear adaptive trajectory tracking control for a stratospheric airship with parametric uncertainty. *Nonlinear Dynamics*, 82(3):1419–1430, 2015.
- [38] D. Wang and C. B. Low. Modeling and analysis of skidding and slipping in wheeled mobile robots: Control design perspective. *IEEE Transactions on Robotics*, 24(3):676–687, June 2008.
- [39] Honglin Wang and Mou Chen. Trajectory tracking control for an indoor quadrotor uav based on the disturbance observer. *Transactions of the Institute of Measurement and Control*, 38(6):675–692, 2016.
- [40] M. S. Wiig, K. Y. Pettersen, and T. R. Krogstad. A 3d reactive collision avoidance algorithm for nonholonomic vehicles. In *2018 IEEE Conference on Control Technology and Applications (CCTA)*, pages 67–74, Aug 2018.
- [41] Haitong Xu, Thor I. Fossen, and Carlos Guedes Soares. Uniformly semiglobally exponential stability of vector field guidance law and autopilot for path-following. *European Journal of Control*, 2019.
- [42] W. Xue et al. Add-on module of Active Disturbance Rejection for set-point tracking of motion control systems. *IEEE Trans. Ind. Appl.*, 53(4):4028–4040, 2017.
- [43] Yueneng Yang and Ye Yan. Neural network gain-scheduling sliding mode control for three-dimensional trajectory tracking of robotic airships. *Proceedings of the Institution of Mechanical Engineers, Part I: Journal of Systems and Control Engineering*, 229(6):529–540, 2015.
- [44] W. Yao, Y. A. Kapitanyuk, and M. Cao. Robotic path following in 3d using a guiding vector field. In *2018 IEEE Conference on Decision and Control (CDC)*, pages 4475–4480, Dec 2018.
- [45] Zewei Zheng and Lihua Xie. Finite-time path following control for a stratospheric airship with input saturation and error constraint. *International Journal of Control*, 92(2):368–393, 2019.
- [46] E. Zhu, J. Pang, N. Sun, H. Gao, Q. Sun, and Z. Chen. Airship horizontal trajectory tracking control based on Active Disturbance Rejection Control (ADRC). *Nonlinear Dynamics*, 75(4):725–734, 2013.